Fisheries and Oceans Canada | Pêches et Océans Canada
Ecosystems and Oceans Science | Sciences des écosystèmes et des océans

Canadian Science Advisory Secretariat (CSAS)

Research Document 2023/068

Quebec Region

Estimating Abundance of Northwest Atlantic Harp Seal Using a Bayesian Modelling Approach

M. Tim. Tinker[1], Garry B. Stenson[2], Arnaud Mosnier[3] and Mike O. Hammill[3]

[1] Nhydra Ecological Consulting,
St. Margaret's Bay, NS B3Z 2G6.

[2] Fisheries and Oceans Canada
Science Branch
P.O. Box 5667
St. John's, Newfoundland A1C 5X1

[3] Maurice Lamontagne Institute
Fisheries and Oceans Canada
850, route de la Mer
Mont-Joli, Québec, G5H 3Z4

December 2023

Canada

Foreword

This series documents the scientific basis for the evaluation of aquatic resources and ecosystems in Canada. As such, it addresses the issues of the day in the time frames required and the documents it contains are not intended as definitive statements on the subjects addressed but rather as progress reports on ongoing investigations.

Published by:

Fisheries and Oceans Canada
Canadian Science Advisory Secretariat
200 Kent Street
Ottawa ON K1A 0E6

http://www.dfo-mpo.gc.ca/csas-sccs/
csas-sccs@dfo-mpo.gc.ca

ISSN 1919-5044
ISBN 978-0-660-68920-3 Cat. No. Fs70-5/2023-068E-PDF

Correct citation for this publication:

Tinker, M.T., Stenson, G.B., Mosnier, A., and Hammill, M.O. 2023. Estimating Abundance of Northwest Atlantic Harp Seal Using a Bayesian Modelling Approach. DFO Can. Sci. Advis. Sec. Res. Doc. 2023/068. iv + 56 p.

Aussi disponible en français :

Tinker, M.T., Stenson, G.B., Mosnier, A., et Hammill, M.O. 2023. Estimation de l'abonde des phoques du Groenland de l'Atlantique Nord-Ouest à l'aide d'une approche de modélisation bayésienne. Secr. can. des avis sci. du MPO. Doc. de rech. 2023/068. iv + 60 p.

TABLE OF CONTENTS

ABSTRACT

In a recent review of the status of the Northwest Atlantic harp seal population, model fit to aerial survey estimates of pup production and annual reproductive rates was poor compared to previous assessments indicating underlying problems relating to model assumptions and/or structure. In this study, a new hierarchical Bayesian state-space model was fitted to the same data on pup production, annual fecundity, human removals, and environmental conditions used in the previous assessment to produce annual estimates of pup production and total abundance from 1952–2019. Data on age structure based upon random samples were also included, and the process model incorporated environmental stochasticity and several other improvements. The new model estimates were similar to the previous model through 1990 but then diverged, indicating that the population peaked in 1997 at 6.6 million animals, almost a decade earlier than modelled in previous assessments. After a period of decline due to high catches and poor ice conditions, the new model provides an abundance estimate of 4.7 (95% Credibility Interval (CI) 3.7-5.7) million in 2019, compared to an estimate of 7.6 (95% CI 6.6-8.8) million in the last assessment. The lower estimates of recent abundance reflect higher and more variable juvenile mortality after 2000 due to a combination of density-dependent and density independent factors operating on juvenile survival. The new model also suggests a decline in equilibrium abundance (K) levels from 7.6 (95% CI=7.4 to 7.8) million Northwest Atlantic harp seals prior to 2000 to 6.8 (95% CI=6.7 to 6.9) million animals post-2000.

Key words: harp seal, *Pagophilous groenlandicus*, abundance, climate change, Bayesian model, population dynamics, pup production.

INTRODUCTION

The harp seal (*Pagophilus groenlandicus*) is a medium sized, migratory phocid distributed over continental shelf regions of the north Atlantic. They are the most abundant pinniped in the North Atlantic (Hammill and Stenson 2022). The Northwest Atlantic (NWA) population, is one of three populations found in this area and is much larger than the other two populations (Greenland Sea and White Sea populations), which number less than 2 million combined (Stenson et al. 2020b).

The NWA population summers in the eastern Canadian Arctic and adjacent waters, but migrates south along the Canadian continental coast in the fall to overwinter and reproduce off northeastern Newfoundland and in the Gulf of St. Lawrence (Figure 1)(Sergeant 1991; Stenson and Hammill 2014). Harp seals require pack ice as a platform, to give birth and nurse their pup. After weaning the young harp seal, now moulted and referred to as a beater, uses the ice as a resting platform for several weeks. Harp seals are harvested commercially mainly during their first year (referred to as Young of the Year or YOY). They are also taken as bycatch in commercial fisheries (Stenson and Upward 2020).

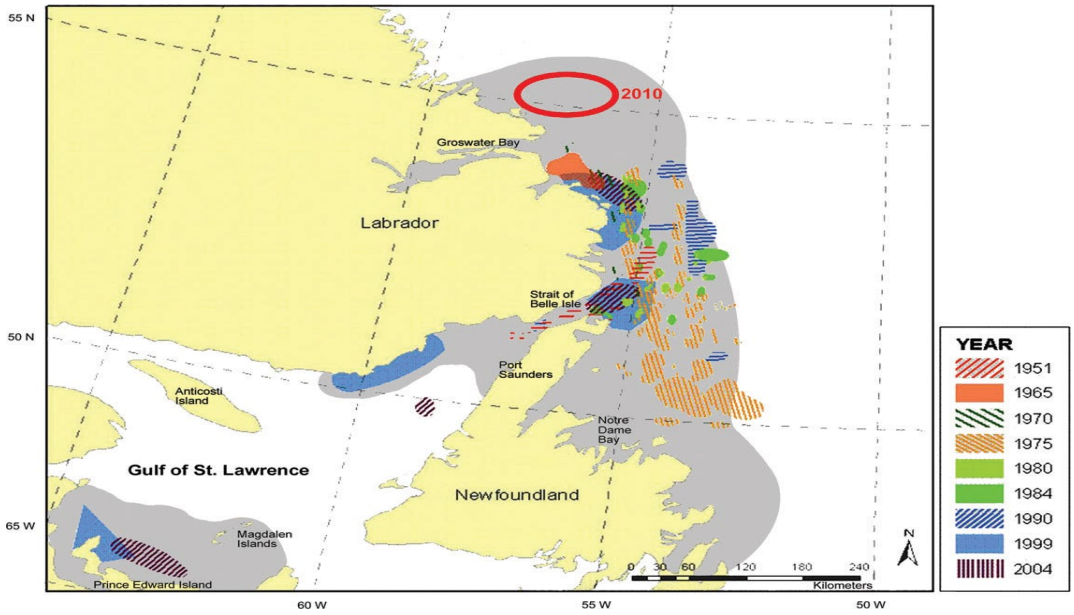

Figure 1. Map of study area showing locations of harp seal whelping patches in the Northwest Atlantic (Stenson and Hammill 2014).

Reproduction and abundance of NWA harp seals have been studied extensively since the 1950s (e.g. Fisher 1954; Sergeant and Fisher 1960; Sergeant 1975; Bowen et al. 1981; Bowen and Sergeant 1983; Myers and Bowen 1989; Sergeant 1991; Sjare et al. 2000; Stenson and Hammill 2014; Stenson et al. 2014, 2016, 2020a). For the past 50 years, the population dynamics, and total allowable catch (TAC), have been estimated using variations of an age-structured deterministic demographic model (Shelton et al. 1992; Healey and Stenson 2000; Stenson et al. 2003, Hammill and Stenson 2010, Stenson and Hammill 2014). This three-parameter population model (referred to as the 'Deterministic Model') was fitted to independent field estimates of pup production and age specific reproductive rates taking into account annual removals from the population. More recently it has also included environmental conditions that are believed to influence the dynamics of the NWA harp seal population (Hammill et al. 2014, 2015, 2021). The basic structure consisted of a discrete-time process model describing annual

reproductive output and survival of 27 age classes: young-of-the year (YOY) , single year age classes from age 1 year up to age 25 years, with all older animals combined into a 26+ class. Animals aged 8 years and older were pooled and assigned a reproductive rate corresponding to the pooled estimate.

Several sources of mortality were included in the process model, including baseline mortality (age class 0 and seals one year of age and older [1+]), density-dependent effects, YOY mortality in whelping patches due to reduced ice cover conditions, and various sources of human removals including reported harvest, bycatch, and the number of seals killed but not landed during the hunt (i.e. struck and lost) in both Canada and Greenland. The unknown parameters that determine process model dynamics were estimated by fitting to observed data sets on pup counts and female pregnancy rates; no survey data are available on abundance of the adult population.

The Deterministic model was relatively successful at predicting pup estimates through the early 2000s; however, from the mid-2000's through 2019, the model was less successful at capturing observed variation in estimates of pup production and showed marked changes in the pattern and trend in abundance compared to earlier evaluations (Figure 2A). Fitting the model to the 1952-2014 data showed a population recovering slowly from 1972 to approximately 1982, then increasing rapidly, peaking at 7.8 million animals in 2008 before declining slightly to 7.4 million animals in 2014 (Hammill et al. 2015). Fitting the model to the new survey estimate of pup production from 2017, and updated reproductive rate and removal data to 2019 provided a very different view of the population trend with recovery beginning from a higher level in 1972 and continuing until 1982, then increasing rapidly to peak at approximately 5.5 million in 1997, leveling off at that level until 2010 when a slight dip was observed, and then a period of renewed growth to 7.6 million animals by 2019 (Hammill et al. 2021; Figure 2B).

Several reasons for model projection discrepancies have been suggested, including greater variability in ice cover and environmental conditions in recent years that may be affecting both pregnancy rates and juvenile survival, as well as limitations in model structure. Some of the structural limitations of the Deterministic model include: 1) lack of formal consideration or inclusion of environmental stochasticity within the process model, particularly in the case of juvenile survival rates and pregnancy rates. Variation in pregnancy rates are allowed for but are not estimated as part of model fitting, rather they are computed separately using a non-parametric smoothing algorithm that prevents disentanglement of observer error and process error; 2) an assumed, fixed (literature-based) ratio of juvenile survival to adult survival rates, and lack of age variation in adult survival (Hammill et al. 2015). In Hammill et al. (2021), this assumption was relaxed slightly by fixing adult survival rate and then allowing the model to estimate a constant juvenile survival rate over the time series; 3) fixed and ad-hoc values for several other model parameters, including density-dependent function shape for juvenile survival and reproductive rates and mortality from ice cover anomalies; 4) model fitting methods that do not allow for separation of variance due to process error and observer error.

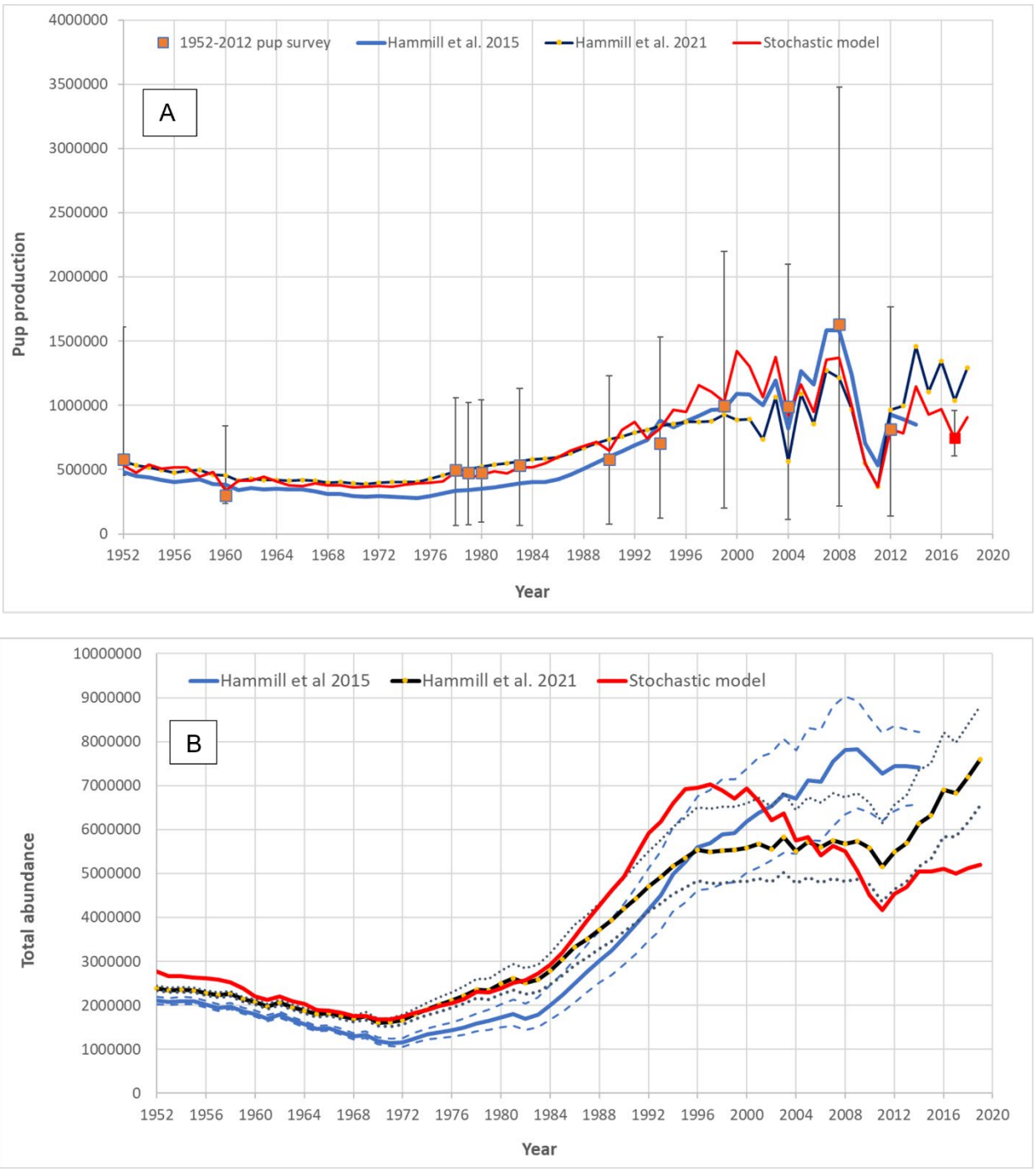

Figure 2. (A) Estimates of pup production from aerial surveys or mark-recapture studies (squares with 95% CI): estimates of pup production from model fit to 1952-2012 survey/mark-recapture estimates, 1952-2014 reproductive rate and removal data (blue line) (Hammill et al. 2015); estimated pup production after model fitted to 1952-2017 survey data, 1952-2019 reproductive rate data and removal data (black line with yellow dots)(Hammill et al. 2021). (B) Estimates of total abundance of northwest Atlantic harp seals fitting the model to aerial survey and reproductive rate data from 1952-2012 survey and projected forward using the 2014 reproductive rate data (blue line) (Hammill et al. 2015); and model fitted to 1952-2017 survey data and reproductive data to 2019 (black line with yellow dots) (Hammill et al. 2021). Dotted lines are 95% Confidence Intervals (95% CI).

This study presents a Stochastic model for the analysis of harp seal demography and population dynamics, fit to the same data sets as presented at the 2019 assessment (Hammill et al. 2021) plus an additional data set on annual age structure of randomly sampled animals. The Stochastic model structure resembles the Deterministic model, in that the process model tracks annual fecundity, survival, and abundance of multiple age classes. However, instead of treating certain parameters as fixed constants, the model attempts to estimate parameter values allowing for data-driven estimates of age specific survival, density-dependent effects, mortality from ice anomalies, and effects of environmental conditions on fecundity and survival. Model fitting is conducted using a hierarchical Bayesian state-space approach that allows for more robust characterization of uncertainty, disentanglement of process error from observer error, and incorporation of multiple data sources with different distributions and variance structures (Buckland et al. 2004, Wang 2009, Williams et al. 2017).

METHODS

This section first presents the inputs to the population model, followed by an explanation of the model structure and fitting. Model performance is evaluated over the period 1952-2019, the same period that was evaluated at the last assessment and, where possible, using the same data.

DATA INPUT

Pup production estimates

The model is fit to 13 independent estimates of pup production, derived using a combination of mark-recapture (m-r) and aerial-survey methods (Table 1) as described in Hammill et al. (2021). The standard errors associated with the four m-r estimates have been doubled following Roff and Bowen (1986).

Table 1. Pup production estimates (SE) from aerial surveys (1951, 1960, 1990-2012), and mark-recapture studies (1978-1983) used as input into the population model (Hammill et al. 2021).

Year	Southern Gulf	Northern Gulf	Front	Total	Method	Reference
1951	-	-	-	645,000 (322,500) *	Aerial survey	Sergeant and Fisher 1960
1960	-	-	-	235,000 (117,500) *	Aerial survey	Sergeant and Fisher 1960
1978	-	-	-	497,000 (68,000) **	Mark-Recapture	Roff and Bowen 1986
1979	-	-	-	478,000 (70,000) **	Mark-Recapture	Roff and Bowen 1986
1980	-	-	-	475,000 (94,000) **	Mark-Recapture	Roff and Bowen 1986
1983	-	-	-	534,000 (66,000) **	Mark-Recapture	Roff and Bowen 1986
1990	106,000 (23,000)	4400 (1,300)	467,000 (31,000)	577,900 (38,800)	Aerial survey	Stenson et al. 1993
1994	198,600 (24,200)	57,600 (13,700)	446,700 (57,200)	702,900 (63,600)	Aerial survey	Stenson et al. 2002
1999	176,200 (25,400)	82,600 (22,500)	739,100 (96,300)	997,900 (102,100)	Aerial survey	Stenson et al. 2003
2004	261,000 (25,700)	89,600 (22,500)	640,800 (46,900)	991,400 (58,200)	Aerial survey	Stenson et al. 2014
2008	287,000 (27,600)	172,600 (22,300)	1,185,000 (112,000)	1,644,500 (117,900)	Aerial survey	Stenson et al. 2014
2012	121,500 (15,300)	74,100 (12 400)	626,200 (66,700)	815,900 (69,500)	Aerial survey	Stenson et al. 2020b
2017	18,300 (1,500)	13,600 (3000)	714,600 (89,700)	746,500 (89,800)	Aerial survey	Stenson et al. 2020b

* Assumed a coefficient of variation of 50% as discussed in Hammill et al. (2021).

** Standard errors have been doubled after Roff and Bowen 1986.

Reproductive rates

Female reproduction rates at age were determined using reproductive tracts and jaws from harp seals sampled around Newfoundland and southern Labrador since 1979 (Stenson et al. 2020b)(Appendix 1, Table A1.1). Sampling has focused upon a core area along the northeast coast of Newfoundland which is adjacent to key winter and spring feeding habitat. Samples were collected by Department of Fisheries and Oceans (DFO) personnel and experienced seal hunters under licenses issued by DFO. To minimize potential sampling biases among years, a core group of hunters from different areas of the province obtained a sample of seals over the entire period.

Ages were determined to the nearest year by sectioning a lower canine tooth and counting dentine annuli (Fisher 1954; Bowen and Sergeant 1983, Frie et al. 2011). Females were considered immature if the ovaries were small and contained only inactive follicles with no corpus luteum (CL) or corpus albicans (CA) (Fisher 1954; Bowen et al. 1981; Stenson et al. 2016). If there was evidence of a CL and/or CA in either ovary, the seal was considered mature. Mature females were considered pregnant if the ovary contained a large, fully luteinized CL in one of the ovaries and, since 1985, the presence of a foetus. Mature females lacking an active CL, but showing evidence of having ovulated previously (i.e., a CA was present) were considered non-pregnant. As in previous studies, all seals less than three years of age were considered immature (Sjare and Stenson 2010; Stenson et al. 2020a).

For ovaries collected after 1984, the size of all CA and CL were measured in two directions and the mean recorded. For ovaries prior to 1985, the maximum diameter was recorded. Seals that lacked a developing foetus but had a CL $\geq$13 mm or CA $\geq$12 mm, a rugose uterus and a large difference in uterine horn width (~15.0 mm), were assumed to have pupped recently (i.e., less than a month, Stenson et al. 2016). For seals collected prior to February 20th, it was assumed that those pups did not survive and that this represented a premature birth (i.e., late-term abortion). For seals collected after February 20th, it was assumed that these pups contributed to the population that year. It is also assumed that if a female has an active CL and foetus on the day of collection, she would have completed the pregnancy successfully.

Fecundity rates, defined as the proportion of mature females that are pregnant, and ag- specific pregnancy rates were calculated as per Stenson et al. (2016). Late-term pregnancy, fecundity, and abortion rates were estimated from seals collected between October and February although the vast majority of seals were collected after November.

Age Structure

Age data were obtained from seals collected for reproductive rates (described above) or during other sampling programs carried out by DFO. Seals of all ages have been collected although there was a suggestion that younger ages may be under, or over, represented in some annual samples. Changes in demographic rates from density dependent and environmental factors are likely to act first on younger age classes (Eberhardt 2002), and thus excluding younger ages limits the ability of the model to capture key demographic trends, especially over the last 5-10 years of the time series. We therefore examined the impact on model results of including younger age classes in model fitting, and then used information theoretical methods to select the optimal minimum age for inclusion (see section on “Model Fitting”, and Appendix 2, for details of minimum age evaluation). Based on this analysis it was determined that using age data for seals 5 years old and above provided the most reliable results.

Catches

The sources of mortality directly due to humans are the commercial and personal use seal hunt in two areas of Atlantic Canada (referred to as 'Front' and 'Gulf'), the subsistence/commercial harvests in Greenland and the Canadian Arctic, and incidental catches in commercial fishing gear (i.e., bycatch). Data on the levels of various components of this mortality are available since 1952 (Stenson and Upward 2020). Because there is normally a two year delay in the collection of the Greenland harvest data, for 2018 and 2019, the average catch for the last five years is used. The reported and estimated catches used in Hammill et al. (2021) are from Stenson and Upward (2020) and are listed in Appendix 3 (Table A3.1). In the past, it has been assumed that catches have been known without error. However, 100% reporting from all of the different sources of human related mortality is unlikely. The impact of different coefficients of variation (CV) in reported mortality (CV=0, 5, 10 and 20%) on model parameter estimates and trend were examined, but there was no evident impact (Appendix 4). Recognizing that there is some uncertainty in total removals, a CV of 10% is assumed.

Corrections for struck and loss are incorporated into the model as the proportion of animals killed that are recovered (Sjare and Stenson 2002). For the whitecoat hunt prior to 1983, the struck and loss correction is only 1%. Since 1983, it is assumed that 95% of the YOY and 50% of the 1+ animals in the Canadian commercial hunt (Front and Gulf) are recovered and reported, while 50% of all animals killed in Greenland and the Canadian Arctic are assumed to have been recovered and reported (Sjare and Stenson 2002)(Figure 3).

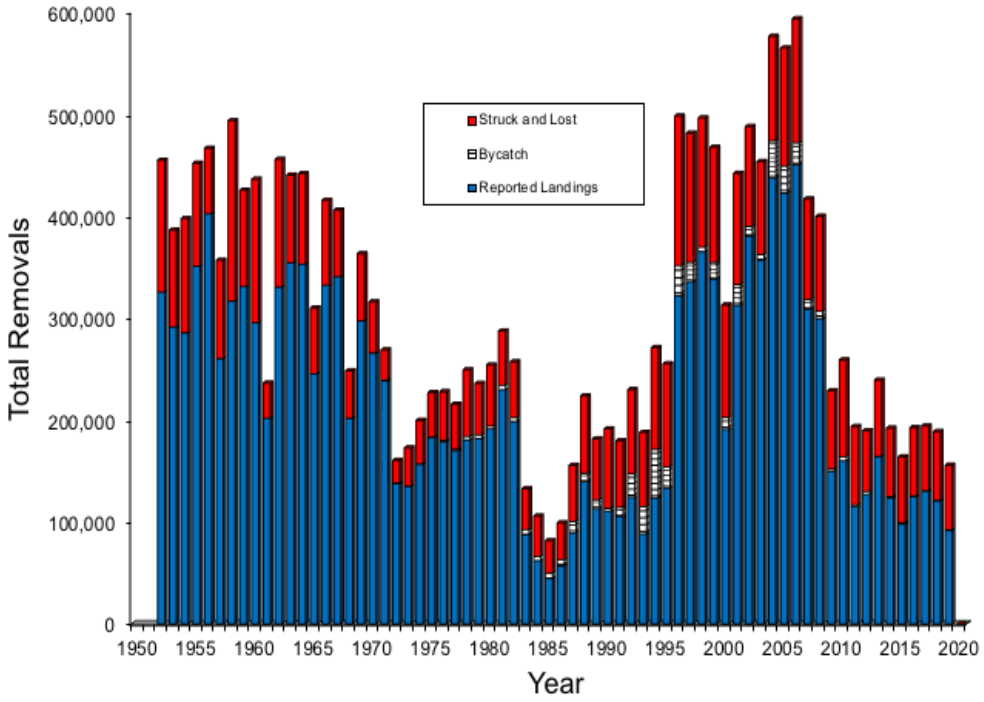

Figure 3. Estimated total human-induced mortality of Northwest Atlantic harp seals (Stenson and Upward 2020). Reported catches from harvesting are adjusted for struck and loss after Sjare and Stenson (2002).

Ice-related mortality of YOY

Poor ice conditions result in increased mortality of YOY during their first month of life (M_{ice})., This mortality is episodic and thus is not captured by the model estimate of average mortality (Stenson and Hammill 2014). Harp seals do not use all of the available ice in the pupping areas

and so minor positive or negative anomalies are unlikely to have an impact on pup survival. However, in some years large numbers of dead pups wash up on the beach, or are observed floating in the water, suggesting higher than usual mortality has occurred. In the previous model we used these observed patterns of mortality to identify a threshold for the values of "ice anomalies" (deviations from average ice cover) likely to result in increased juvenile mortality in the Gulf and at the Front (Hammill et al. 2021). There has been an overall decline in ice cover in both regions since the late 1990s. A standard ice cover anomaly was developed using the average ice cover between 1969-2000 (Figure 4; see below). The annual ice anomaly (*IC*) was calculated using the formula: $IC_t = (ice\ cover_{\ t} - ice\ cover_{\ mean\ 1969\text{-}2000}) / ice\ cover_{\ mean\ 1969\text{-}2000}$ where ice cover is in km^2 in year *t*. Total first year ice (the type primarily used for pupping) extent was extracted from the Gulf of St. Lawrence and southern Labrador ice charts for the weeks of 28 February and 5 March respectively (Canadian Ice Service of Environment Canada).

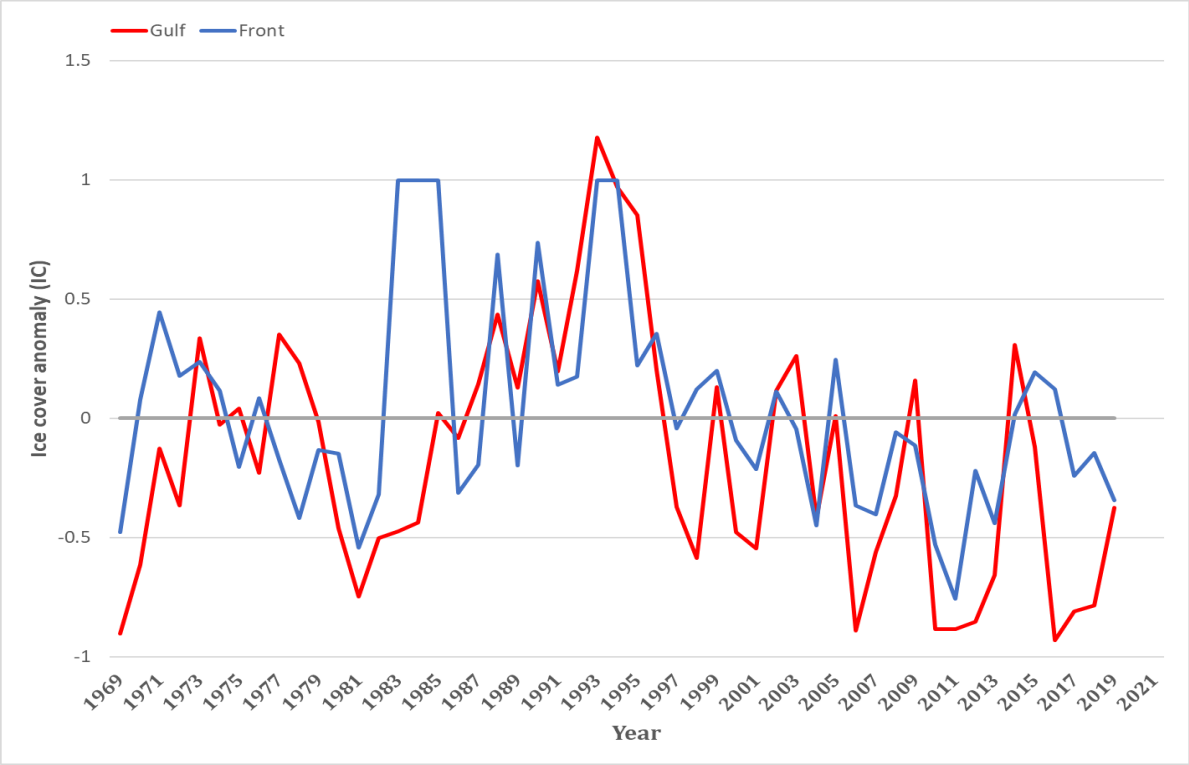

Figure 4. Ice anomalies using mean first-year ice cover during 1969-2000 as the baseline year. The annual ice anomaly (IC) was calculated using the formula: $IC_t = (ice\ cover_{\ t} - ice\ cover_{\ mean\ 1969\text{-}2000}) / ice\ cover_{\ mean\ 1969\text{-}2000}$ where ice cover is in km^2 in year t. Data from the Canadian Ice Service of Environment and Climate Change Canada for the areas Gulf of St Lawrence and southern Labrador.

In Hammill et al. (2021), no additional mortality was assumed to occur if the ice-cover anomaly was at or above the threshold (where threshold ice cover =-0.3 in Gulf, and -0.5 at Front), but if the anomaly was below the threshold, higher than normal mortality was assumed to be proportional to the magnitude of the negative anomaly. Thus a 60% decline in ice cover was assumed to result in 60% mortality (or 40% survival). M_{ice} was calculated for the Front and the Gulf separately and then the two indices were combined, weighted assuming that 30% of pups are born in the Gulf and 70% at the Front. These were converted to a survival index (S_{ice}=1-$M_{ice;}$). In the Stochastic model, the same ice anomaly index values were used, but no assumptions were made about the magnitude of associated mortality; rather, the functional relationship between ice anomalies and juvenile survival was estimated as part of model fitting.

Comprehensive Environmental Index (Newfoundland Climate Index)

To account for some ecosystem variability a Comprehensive Environmental Index has been incorporated into the model as a multiplier on ecosystem carrying capacity (K) (Hammill et al. 2021). The Comprehensive Environmental Index (CEI) provides a measure of the overall state of environmental conditions. The index is a mosaic of a time series including meteorological, sea temperature, salinity, ice and cold intermediate layer measurements from a variety of sites in the Northwest Atlantic. It is calculated annually as the sum of the standardized anomalies of 28 environmental indices (Colbourne et al. 2016). Negative values generally reflect cooler conditions while positive values reflect warmer (Figure 5). Because of difference data availability among some of the measures and potential duplication, the Comprehensive Environmental Index has been revised, updated and renamed the Newfoundland Climate Index (Figure 5, Cyr and Galbraith 2021). The Newfoundland climate Index (NCI) uses a reduced number of components (10) and is calculated as the average of the different components rather than their sum.

Hammill et al. (2021) used the CEI in their analysis while in this analysis, the NCI is used. The two indices are very similar (correlation 0.86). Lower values are associated with cooler conditions, considered more favourable to harp seals, whereas higher values are associated with warmer conditions.

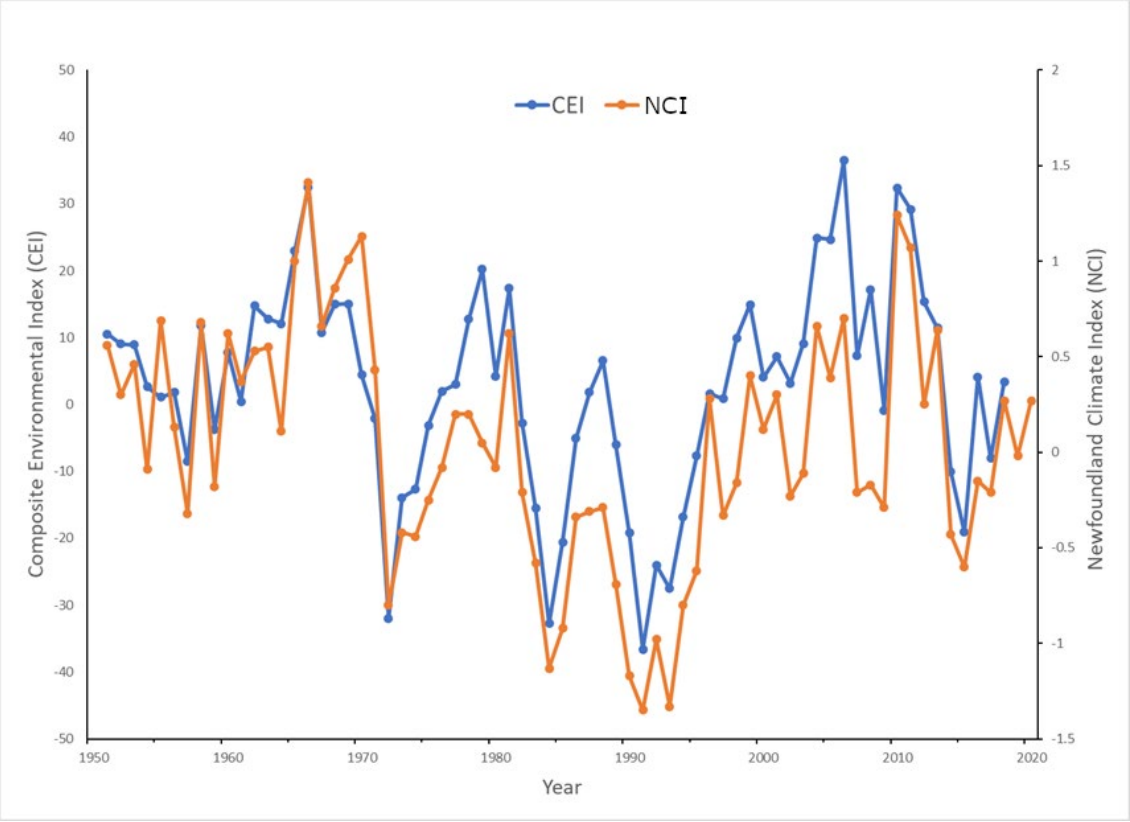

Figure 5. Variability in the Comprehensive Environmental Index (CEI) between 1950 and 2018 used in Hammill et al. (2021). The CEI has been replaced by the Newfoundland Climate Index (NCI) developed by Cyr and Galbraith (2021). There is strong correlation between the two indices.

MODEL DESCRIPTION

The methods for analyzing the harp seal population can be described in three parts: 1) the process model, a series of equations that describe demographic transitions and which, when solved, predict dynamics in the variables of interest (e.g. population abundance) based on the values of the input parameters; 2) the data model, which describes how empirical data sets are related to the predicted dynamics of the process model; 3) model fitting, which describes how input parameters are estimated. All parameters estimated by model fitting are summarized in Table 2.

PROCESS MODEL

Population dynamics are described using discrete annual time steps and formulated assuming a pre-breeding estimate (i.e. the population state at time *t* corresponds to the state at the beginning of a pupping season), as this formulation simplified interpretation of age samples and pregnancy rate data (pup counts could then be compared with expected births given number of pregnant animals. Model terms are presented in Table 2. The population is age-structured, such that a population vector *n*(*i,t*) describes the number of individuals in age class *i* (*i* = 1, 2… 36) at year *t*, and *N*(*t*) is the sum of *n*(*i,t*) across age classes. We note that the last age class, *i* = 36, represents a multi-year class comprised of all animals older than 35 yrs; also, we assume a 50:50 sex ratio for all age classes (i.e., we assume survival rates are similar for males and females, as harp seals do not show pronounced sexual dimorphism). Under the assumption of a pre-breeding abundance estimate the first entry in the population vector (*n*(1,*t*)) represents juveniles (age class 0) about to recruit to the adult (seals one year of age and older or 1+) population (i.e., pups born the previous year that have survived to just before their first birthday), although we note that the model also tracks YOY as the summed reproductive output of adults. Demographic transitions from year *t* to year *t+1* are calculated from annually varying vital rates, including fecundity (*F*), juvenile survival (S_0, the probability a pup survives from weaning to its first birthday), and adult (1+) survival ($S_A(i)$, the probability an individual of age *i,* where *i* is ≥1, survives to the next year). Vital rates are assumed to be density-dependent, meaning that they can vary as functions of relative population abundance (*N*, which for computational tractability we re-scale to units of millions of animals, *N**) and are also affected by annually varying environmental conditions, ice cover and harvest/bycatch mortality (Hammill and Sauvé 2017).

Fecundity

The factors that determine the probability that a female gives birth (or at least reaches late-stage pregnancy) at year *t* are her age (*i*), current population abundance (N*(t)), environmental and climatic conditions (NCI), and unexplained variance or environmental stochasticity (ε_F(Stenson and Hammill 2014). Fecundity is fixed at 0 for females aged 1-3 years, and is calculated using a logit function for females > 4 years:

$$logit\big(F(i,t)\big) = \beta_1 + \beta_2 \cdot (8-i)^2 - \big(\emptyset_F \cdot N^*(t)\big)^{\theta_F} - \delta_F \cdot NCI(t-1) + \varepsilon_F(t) \quad (1)$$

where stochasticity in pregnancy rates (ε_F) is modeled as a hierarchical effect and estimated as:

$$\varepsilon_F(t) \sim normal(0, \sigma_F) \quad (1)$$

and where β, ϕ_F, θ_F, δ_F, and σ_F are all parameters to be estimated from the observed late term pregnancy rates. The direction and magnitude of effects on fecundity associated with the NCI are determined by parameter δ_F, and we assume a 1-year lag (i.e., female fecundity in year *t* is primarily affected by the NCI value in year *t*-1). Equation (1) also includes density-dependent effects (determined by current population abundance and parameters ϕ_F and θ_F), and age

effects are structured such that fecundity becomes asymptotic by age 8 (annual fecundity for females aged >8 years is set equal to $F(8,t)$) following previous analyses (Stenson et al. 2003).

Survival from competing hazards: overview

We use a proportional hazards formulation to model survival, which provides a mathematically coherent way to incorporate and estimate multiple competing hazards. Expressed in a slightly different way, a cause-specific hazard represents the instantaneous risk of dying from a specified cause. The cumulative hazards function is a mathematical expression that defines the total probability of dying at time t from all sources of mortality (e.g., Gelfand et al. 2000, Heisey and Patterson 2006, Beyersmann et al. 2009, Brodie et al. 2013). Specifically, the cause-specific hazards we wish to estimate include harvest/bycatch mortality, hazards associated with anomalously low ice cover (for juveniles), and baseline hazards including density dependence and additional unexplained environmental stochasticity. In the following paragraphs we describe how each of these hazards are estimated and then combined to derive annual survival rates for juveniles and adults. Note that when fitting hazards models, it is typical to work with log-transformed hazard rates (represented by the symbol γ), as this allows various fixed and random effects to be expressed as simple additive equations.

Age-specific baseline hazards

Baseline hazards are assumed to represent all sources of "natural mortality" (excluding the mortality of pups from anomalously low ice cover, which is calculated as a separate hazard as described below) and incorporate density-dependence and environmental stochasticity. We assume that baseline hazards can vary with age in a non-linear manner (i.e. the typical "U-shaped" pattern of age-specific mortality for many mammals; Caughley 1966; Chu et al. 2007), and thus express the age-varying component of baseline log-hazards as:

$$\gamma_A(i) = \alpha_0 - \alpha_1 \cdot \max(0,10 - i) + \alpha_2 \cdot \max(0, i - 10)^2 \quad (2)$$

Note that we re-center the age vector in equation 3 by subtracting 10 to simplify fitting and parameter interpretation: specifically, α_0 represents baseline log hazards for a 10 yr-old adult, α_1 represents additional log hazards for younger animals and α_2 represents additional log hazards for older animals. For juveniles (γ_0) we solve the same equation with $i = 0$.

We also allow for effects of density-dependence and, for juveniles, environmental variation as captured by the NCI, as well as additional unexplained stochasticity. Density-dependent log-hazards were calculated as a function of current population abundance (similar in form to density-dependent effects on fecundity):

$$\gamma_D = (\emptyset_S \cdot N^*(t))^{\theta S} \quad (3)$$

The direction and magnitude of effects associated with climate-driven variation are calculated analogously to the formulation for fecundity (but with no lag, thus assuming that current-year conditions affect juvenile survival), as $\delta_S \cdot NCI$. Environmental stochasticity in survival ($\varepsilon_S(t)$) is modeled as a random hierarchical effect:

$$\varepsilon_S(t) \sim normal(0, \sigma_S) \quad (4)$$

We sum the log-hazard effects described in equations 3–5 and transform by exponentiation to derive the baseline hazard terms for juveniles and adults:

$$h_0(t) = \exp(\omega + \gamma_0 + \gamma_D + \delta_S \cdot NCI(t) + \varepsilon_S(t)) \quad (5)$$

$$h_A(i,t) = \exp(\omega + \gamma_A(i) + \left(\frac{1}{i+0.5}\right)^{\zeta} \cdot \gamma_D) \quad (6)$$

Where parameters α_0, α_1, α_2, ϕ_S, θ_S δ_S, ζ and σ_S are all estimated as part of model fitting, and ω is a nuisance constant (arbitrarily fixed at -7) that improves fitting and simplifies interpretation by allowing all other log-hazard parameters to represent log hazard ratios relative to a minimum possible mortality rate. We note that variation due to NCI and stochastic effects for adults is assumed to be minor and thus safely omitted from equation (7), while density-dependent effects are assumed to be small relative to juveniles and to vary with age, with parameter ζ controlling the rate at which density-dependent effects on survival decline with age.

Ice anomaly hazards (juveniles)

One potential source of mortality for pups in the juvenile age class (age 0) is associated with poor ice conditions, which can lead to drowning of juveniles when ice breaks up during storms. While impossible to predict such events with certainty, they are more likely to occur during years with relatively low ice cover. The model tracks this ice-related mortality as a separate hazard for juveniles, modelled as a function of an "Ice Anomaly index" (*IC*). The IC is calculated for each year (*t*) and breeding area (*a*) as the proportional deviation in % first-year ice from the average % first-year ice cover for breeding area *a* over the period 1969-2000 during the weeks of Feb 26 in the Gulf and March 5 at the Front which corresponds to the beginning of pupping in the two areas, where:

$$IC(a,t) = \%icecov(a,t) - {avg.[\%icecov(a)]}\Big/{avg.[\%icecov(a)]} \quad (7)$$

The *IC* index thus varies between 1 and -1, with 0 corresponding to the average of ice cover between 1969 and 2000 (Hammill et al. 2014). Values significantly less than 0 indicate anomalously low ice cover. The form of the functional relationship between log-hazards from poor ice conditions and *IC* was defined based on the recognition that in years with average or above-average ice cover, there is little or no mortality, but in years when the ice cover is significantly below average the mortality rate increases sharply. Accordingly, we calculate ice-related log hazards for each breeding area and year using a scaled logit function:

$$\gamma_{IC}(a,t) = (-\omega + 1) \cdot inv.logit[\Psi_1 - \Psi_1 \cdot IC(a,t)] \quad (8)$$

where ψ_1 and ψ_2 are estimated parameters and ω is the nuisance constant defined above. Recognizing that ice anomalies in the Gulf and at the Front might have differing effects on juvenile survival, we fit separate values of parameter ψ_1 for the Gulf (ψ_{1G}) and Front (ψ_{1F}). To calculate the population-level hazards from ice anomalies, we transform by exponentiation and take the weighted average across breeding areas (*a* = 1 for S. Gulf, 3 for Front), with weighting determined by the proportion of pups born in each breeding area (*P*(*a*,*t*)):

$$h_{IC}(t) = \sum_{a=1}^{3} P(a,t) \cdot \exp\left(\omega + \gamma_{IC}(a,t)\right) \quad (9)$$

Harvest/by-catch hazards

Cumulative deaths from all human activities– including fishing by-catch, legal harvests of adults and YOY in eastern Canada, the Canadian Arctic, and Greenland, as well as struck and loss mortality from harvests–- are represented in the model as a separate hazards term. The magnitude of these sources of mortality varies from year to year, so we calculate the log-hazards associated with harvest/by-catch for YOY (age 0) and adults (ages>0) as hierarchical random effects:

$$\gamma_{H0}(t) \sim normal(\bar{\gamma}_{H0}, \sigma_H) \quad (10)$$

$$\gamma_{HA}(t) \sim normal(\bar{\gamma}_{HA}, \sigma_H) \quad (11)$$

where the parameters to be fit include average log-hazards from harvest/bycatch for YOY ($\bar{\gamma}_{H0}$), average log-hazards from harvest/bycatch for adults ($\bar{\gamma}_{HA}$) and the magnitude of variance in harvest hazards from year to year (σ_H). We then convert log-hazards to hazard rates by exponentiation:

$$h_{H0}(t) = \exp\left(\omega + \gamma_{H0}(t)\right) \tag{12}$$

$$h_{HA}(t) = \exp\left(\omega + \gamma_{HA}(t)\right) \tag{13}$$

Net annual survival

For both juveniles and adults, annual survival rates represent the joint probability of surviving all competing hazards, and are calculated as:

$$S_0(t) = \exp\left(-1 \cdot [h_0(t) + h_{IC}(t) + h_{H0}(t)]\right) \tag{14}$$

$$S_A(i,t) = \exp\left(-1 \cdot [h_A(i,t) + h_{HA}(t)]\right) \tag{15}$$

We also define an additional constant term for newborn pup survival ($S_{np}(t)$) to account for early pup mortality that occurs prior to the pup counts. Early pup survival is thought to be quite high (Stenson and Hammill, DFO unpublished data), hence we fix S_{np} at 0.95.

Estimated Population dynamics

The estimated vital rates described above (age-specific survival and fecundity) are organized into an age-based projection matrix (Caswell 2001) having dimensions 36×36, that describes all demographic transitions at year *t*:

$$\boldsymbol{M}(t) = \begin{bmatrix} 0 & 0 & 0 & R(4,t) & \cdots & R(35,t) & R(36,t) \\ S_A(1,t) & 0 & 0 & 0 & \cdots & 0 & 0 \\ 0 & S_A(2,t) & 0 & 0 & \cdots & 0 & 0 \\ 0 & 0 & S_A(3,t) & 0 & \cdots & 0 & 0 \\ 0 & 0 & 0 & S_A(4,t) & \cdots & 0 & 0 \\ \vdots & \vdots & \vdots & \vdots & \ddots & \vdots & \vdots \\ 0 & 0 & 0 & 0 & \cdots & S_A(35,t) & S_A(36,t) \end{bmatrix} \tag{16}$$

In projection matrix **M**(*t*), the terms in the first row, *R*(*i, t*), represent reproductive contributions to the juvenile age class (assuming a 50:50 sex ratio) and are calculated as:

$$R(i,t) = \tfrac{1}{2} \cdot F(i,t) \cdot S_{np}(t) \cdot S_0(t) \tag{17}$$

We next define a population vector, **n**(*t*), which describes the number of individuals in each age class *i* at year *t*, such that the sum of **n**(*t*) gives *N*(*t*), total abundance. We can then calculate the expected age vector in the following year, **n**(*t+1*), via matrix multiplication:

$$\boldsymbol{n}(t+1) = \mathbf{M}(t) \times \boldsymbol{n}(t) \tag{18}$$

To initiate the population vector at year 0 we multiply the estimated starting abundance (N_0, a parameter to be fit) by the stationary age distribution (*SAD*) associated with the parameterized demographic schedule at *t* = 1. The *SAD* is calculated iteratively: we arbitrarily specify an initial age distribution, fit the model, algebraically calculate the stable age distribution associated with the parameterized matrix at year 1 (Caswell 2001), re-fit the model using this new initial age distribution, and repeat the process until values stabilize.

Predicted age distribution, pup counts, and harvest/bycatch mortality

The predicted age frequency distribution at year *t* is calculated as:

$$Agedist,pred(t) = \frac{[n(m,t) \quad n(m+1,t) \quad \cdots \quad n(36,t)]}{\sum_{i=m}^{36} n(i,t)} \tag{19}$$

where *m* is the minimum age of adults to be considered for comparison with observed age distributions, and $n(i, t)$ represents the i^{th} element of population vector $\mathbf{n}(t)$.

The predicted number of pups available to be counted during a survey in year *t* is calculated as:

$$Pups.pred(t) = 0.5 \cdot (\sum_{i=1}^{36} n(i,t) \cdot F(i,t)) \cdot S_{np}(t) \tag{20}$$

We note that equation (21) reflects a 50:50 sex ratio and assumes that a small amount of post-birth mortality will have occurred prior to the pup count, as determined by survival term $S_{np}(t)$.

To calculate expected harvest mortality, we first calculate the fraction of all first-year deaths accounted for by harvest or bycatch of YOY in year *t* ($f_{H0}(t)$) based on the ratios of cause-specific hazards:

$$f_{H0}(t) = \frac{h_{H0}(t)}{[h_0(t)=h_{IC}(t)+h_{H0}(t)]} \tag{21}$$

This value is then used to calculate the predicted total harvest/bycatch of YOY in year *t*, after accounting for struck and loss:

$$pred.H_0(t) = Pups.pred(t) \cdot (1 - S_0(t)) \cdot f_{H0}(t) \cdot Q_0(t) \tag{22}$$

where $Q_0(t)$ represents the proportion of harvested YOY that are recovered (i.e., not struck and lost) in year *t*.

Similarly, the fraction of total adult deaths in each age class represented by harvest/bycatch of adults in year *t* is calculated as:

$$f_{HA}(i,t) = \frac{h_{HA}(t)}{[h_A(i,t)+h_{HA}(t)]} \tag{23}$$

We note that this formula implicitly assumes that the harvest-removals for each age class will be proportional to the living age structure (i.e. excluding YOY harvests), and thus does not account for any age bias in harvests. This value is then used to calculate the predicted total harvest/bycatch of adults in year *t*, after accounting for struck and loss:

$$pred.H_A(t) = \sum_{i=1}^{36} n(i,t) \cdot (1 - S_A(i,t)) \cdot f_{HA}(i,t) \cdot Q_A(t) \tag{24}$$

where $Q_A(t)$ is the proportion of harvested adults that are recovered (i.e., not struck and lost) in year *t*.

DATA MODEL

The variables generated by the process model are compared to 4 independent data sets: aerial pup surveys, pregnancy rates of sampled females, age composition of sampled adults, and the combined harvest/bycatch estimates from multiple sources. The pup abundance estimates are assumed to follow a gamma distribution:

$$Pups.obs(t) \sim gamma\left(a = \frac{[Pups.pred(t)]^2}{[SE_p(t)]^2 \cdot exp(\nu)},\ b = \frac{Pups.pred(t)}{[SE_p(t)]^2 \cdot exp(\nu)}\right) \tag{25}$$

where standard error estimates associated with each pup survey (SE_p) were calculated separately [Table 1; Stenson et al. 2014, 2022]. Parameter ν is a variance-adjustment parameter included to facilitate model fitting and improve model goodness of fit.

The data on pregnancy rates of sampled females are treated as a beta-binomial variable: specifically, given a sample of *N* females of age *i* in year *t* ($NF(i, t)$), the number of pregnant

females (*NPr.obs*(*i, t*)) is assumed to follow a beta-binomial distribution with probability determined by the model-estimated fecundity rates, and scale parameter η (such that the distribution converges to a standard binomial distribution as η approaches 0):

$$NPr.obs(i,t) \sim beta - binomial\left(NF(i,t), {}^{1}/_{\eta} \cdot F(i,t), {}^{1}/_{\eta} \cdot [1 - F(i,t)]\right) \quad (26)$$

The age composition data are treated as a multinomial variable. Specifically, samples of adult animals in year *t* were assorted by age into vectors of counts, *Agedist.obs*(*t*) = [*NC*(m,*t*),*NC*(m+1,*t*)… *NC*(*36,t*)], where *m* is the minimum age to be considered. These vectors are assumed to follow a multinomial distribution with frequency distributions corresponding to the model-predicted age distribution vectors ($Agedist.pred(t)$). To account for additional noise and sampling error in the age counts, we use a Dirichlet-multinomial formulation with fitted precision parameter τ:

$$(t) \sim dirichlet(\tau \cdot [Agedist.pred(t)]),$$
$$Agedist.obs(t) \sim multinomial\left(\sum_{i=m}^{36} NC(i,t),\ \pi(t)\right) \quad (27)$$

We used model comparisons of likelihood-based information criteria to determine the best-supported minimum age (see Model fitting section, below).

The summed annual harvest/bycatch estimates are assumed to follow normal distributions:

$$obs.H_0(t) \sim normal(pred.H_0(t), SE_{HV}) \quad (28)$$

$$obs.H_A(t) \sim normal(pred.H_A(t), SE_{HV}) \quad (29)$$

where the standard error values for observed harvest estimates correspond to an assumed CV of 0.1.

Table 2. Summary and descriptions of the parameters included in the model

Parameter		Description
Symbol		Name
N_0		Starting population abundance at *t* = 1 (1952)
β_1	$Beta_1$	Maximum pregnancy rate for adult females (logit transformed)
β_2	$Beta_2$	Age-effect on fecundity (pregnancy rate increases with age up to 8 years)
ϕ_F	Phi_F	Density-dependent effects on fecundity
θ_F	$Theta_F$	Shape-parameter for density-dependent effects on fecundity
δ_F	$Delta_F$	Effect of environmental conditions (NCI index) on fecundity
σ_F	$Sigma_F$	Unexplained variation in annual fecundity
α_0	$Alpha_0$	Intercept for age-varying hazards fxn (10-yr-old log hazards)
α_1	$Alpha_1$	Parameter for age-varying hazards fxn (increased hazards for age <10 years)
α_2	$Alpha_2$	Parameter for age-varying hazards fxn (increased hazards for age >10 years)
ϕ_S	Phi_S	Density-dependent effects on survival (primarily juveniles)
θ_S	$Theta_S$	Shape-parameter for density-dependent effects on survival
δ_S	$Delta_S$	Effect of environmental conditions (NCI index) on juvenile survival
σ_S	$Sigma_S$	Unexplained variation in juvenile survival

Parameter		Description
Symbol		Name
ζ	$Zeta$	Parameter to scale density-dependent effects for adult animals by age
ψ_1	Psi_1	Parameter 1 for fxn describing ice anomaly effects on juvenile mortality
ψ_2	Psi_2	Parameter 2 for fxn describing ice anomaly effects on juvenile mortality
$\bar{\gamma}_{H0}$	$Gamma_{H0}$	Mean log hazard rate for YOY harvest/bycatch mortality
$\bar{\gamma}_{HA}$	$Gamma_{HA}$	Mean log hazard rate for adult (1+ year) harvest/bycatch mortality
σ_H	$Sigma_H$	Unexplained variation in annual log hazard rates for harvest/bycatch mortality
τ	Tau	Precision parameter, Dirichlet-multinomial distribution of age-class samples
ν	Nu	Variance adjustment parameter for gamma distribution of pup counts
η	Eta	Scale parameter for beta-binomial distribution of female pregnancy status

MODEL FITTING

The observed data variables constrain the possible values of unknown parameters in the process model, allowing us to estimate posterior distributions for these parameters using standard Markov Chain Monte Carlo (MCMC) methods. We use vague prior distributions for most parameters (i.e., weakly informed based on biological feasibility but having no information specific to the analysis), including Gamma priors for N_0 and θ, Cauchy priors for unbounded parameters and half-Cauchy priors for parameters that were logically constrained to be positive, including ν, η, τ, and all variance parameters σ (Gelman 2006, Gelman et al. 2008). The Cauchy distribution has been suggested as an effective, uninformative prior because it has a taller peak than the Normal distribution, is leptokurtic (“fat tailed”), and has no defined mean, and thus provides wide potential bounds on parameter space, a tendency to shrink towards 0 for non-significant parameters and minimized influence of the prior on the estimation of the posterior (Gelman et al. 2008). The half-Cauchy distribution is simply a Cauchy distribution that has been truncated to only have nonzero probability density for values greater than the peak (usually 0). For the ice-anomaly effect parameters (ψ_1 and ψ_2) we used weakly-informed normal priors with means of 0 and 4 and standard deviations of 1 and 2 (respectively), as these values produced a broad range of potential functional relationships between ice anomalies and pup mortality that agreed well with existing information on ice-based pup mortality. For average harvest log-hazard ratios ($\bar{\gamma}_{H0}$ and $\bar{\gamma}_{HA}$) we used weakly-informed normal priors with means of 5 and standard deviations of 2.

We used R (R.Core.Team 2022) and Stan software (Carpenter et al. 2017) to code and fit the model, saving 20,000 samples after a burn-in of 1000 samples. We evaluated model convergence by graphical examination of trace plots from 20 independent chains and by ensuring that Gelman-Rubin convergence diagnostic (R-hat) was <1.1. We plotted and visually compared prior and posterior distributions for all parameters to assess the degree to which posteriors were distinct from priors. We conducted graphical posterior predictive checking to evaluate model goodness of fit, ensuring that out-of-sample predictive distributions of pup abundance and female pregnancy rates were consistent with distributions of observed data. We also calculated associated Bayesian-P values (using Pearson residuals as the test statistic to compare for observed vs. out-of-sample predicted data), with good model fit indicated by 0.05 < Bayesian-P < 0.95. As an additional goodness-of-fit check, we created “out-of-sample” hindcast projections of population dynamics to compare to the fitted model projections. Specifically, for

each out-of-sample projection we initiated a "new" 1951 population at N_0, and then projected forward for *T* years with the process model parameterized by drawing from the joint posteriors of all parameters and with random effects drawn randomly from their appropriate sampling distributions (with the exception of harvest-based hazards, which were set to mean estimated values). In the case of a well-fit model, the estimated abundance projection should fall within the distribution of out-of-sample hindcast projections.

We used an information theoretic approach to determine the best-supported minimum age (m) for inclusion in model fitting of age distributions (Equation (28)). We evaluated values of m from 4 to 8 and used R package "Loo" (Vehtari et al. 2017) to calculate the "Leave-one-out cross validation information criterion" (LooIC). We limited LooIC calculations to likelihood posteriors computed from pup counts and pregnancy rate data but excluding age distribution likelihoods (since the number of age classes contributing to age distribution likelihoods differed across models). We then used the Loo package to conduct model comparisons, identifying the best supported model based on the lowest LooIC value or (equivalently) the highest expected log pointwise predictive density (ELPD) for a new data set (Vehtari et al. 2017). The model having the lowest LooIC or highest ELPD is the model most likely to correctly estimate new data points that were not included in model fitting.

Model results are summarized by reporting the mean and 95% Credible Interval (CI) of the posterior distributions for base model parameters (Table 3) and derived parameters. We graphically compare hindcast projections of population abundance, pup production, pregnancy rates and age composition based on the Stochastic model with equivalent estimates based on the Deterministic model.

MODEL SIMULATIONS

We generated projections of future population dynamics under various scenarios by running Monte Carlo simulations of the process model, parameterized by drawing from the joint posteriors of all parameters and with random effects drawn randomly from their appropriate sampling distributions. To estimate functional carrying capacity (*K*), we initiated each of 20,000 simulations with the final estimated population vector (based on model fitting to current data) and projected forward for 100 years, with harvest/bycatch hazards (h_{H0} and h_{HA}) forced to 0. The resulting distribution of simulated trajectories therefore included the effects of ice mortality, environmental/climatic conditions, stochasticity, and density-dependent effects, but not human-caused mortality. The average abundance of these forward simulations generally stabilized after 50 years, so we used the mean values (and 95% CI) of the abundance over the last 50 years of the 100-year time series to estimate equilibrium abundance in the absence of harvest. A key consideration for these future simulations is how environmental conditions and ice cover may change in the future. To explore the potential impacts of changes in these variables, we repeated the carrying capacity simulations under two different scenarios: 1) values of IC and NCI were drawn from their pre-2000 empirical distributions; and 2) values of IC and NCI were drawn from their post-2000 empirical distributions. The second scenario thus assumes that future conditions will be more similar to those observed since 2000 than to earlier conditions. We note that other future scenarios could be explored as well, including scenarios where both ice cover and environmental conditions show continued reductions over time.

RESULTS

The Stochastic model incorporated the age distribution data from the Newfoundland sample collection program into the model structure. Early in the time series, the age structure of this data set was dominated by animals aged 4-7 years, but beginning in the late 1990s, older age

classes sequentially became more important while younger animals comprised a smaller and smaller proportion of the time series, reaching a minimum by 2010. We interpret this as a decline in recruitment to the breeding population (Figure 6). Since 2010 there has been a slight increase in recruitment of younger animals to the sampled age structure, although animals aged 20+ years old continue to dominate the time series.

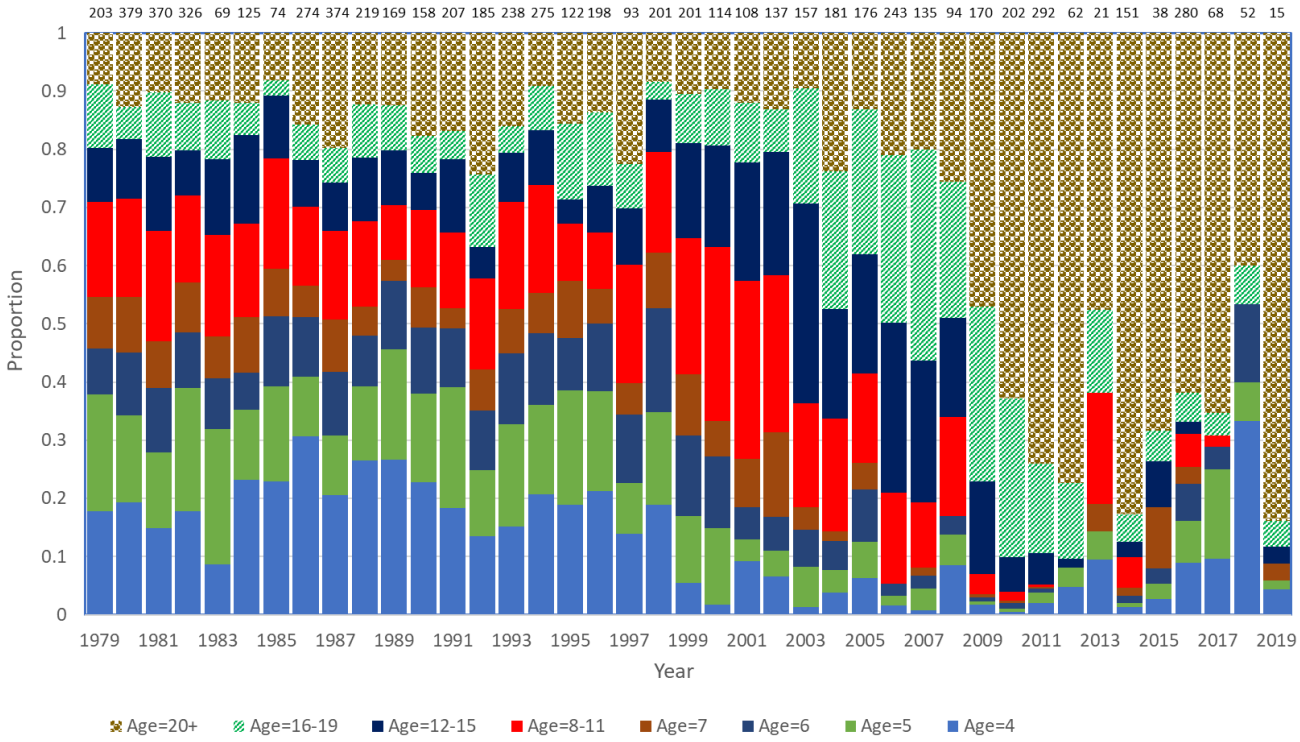

Figure 6. Proportion of samples comprised of different age classes (years) collected by year between 1979-2019. Sample sizes for ages 4 to 20+ years are across the top

Fitting the Stochastic model to the three independent data sets provides excellent convergence, with R-hat<1.1 for all parameters (Table 3). The best supported model included a minimum age (*m*) of 5 (Appendix 2). Graphical posterior predictive checks indicate excellent model fit, with observed data distributions corresponding closely to distributions of out-of-sample projected estimates (Figure 7) and Bayesian-P values of 0.134 and 0.265 for pup counts and pregnancy rate data, respectively. For all parameters the estimated posterior distributions are clearly distinct from prior distributions (Appendix 5).

Table 3. Summary of parameter estimates from model fitting, including the mean, standard deviation and lower/upper 95% quantiles of the posterior distributions. Also shown are r-hat statistics for each parameter, with values close to 1 indicating well mixed chains (and thus model cnvergence). Note that initial population size (N_0) is in millions of animals.

Parameter		Mean	SD	CI95_lo	CI95_hi	r-hat
N_0		2.256	0.155	2.019	2.523	1.031
β_1	$Beta_1$	2.697	0.621	1.759	3.824	1.022
β_2	$Beta_2$	0.273	0.017	0.246	0.302	1.002
ϕ_F	Phi_F	1.098	1.183	0.272	3.348	1.016
θ_F	$Theta_F$	0.739	0.252	0.426	1.219	1.008
δ_F	$Delta_F$	0.299	0.141	0.064	0.533	1.022
σ_F	$Sigma_F$	0.422	0.083	0.287	0.560	1.047
α_0	$Alpha_0$	1.280	0.482	0.415	2.016	1.048
α_1	$Alpha_1$	0.141	0.078	0.022	0.278	1.023
α_2	$Alpha_2$	0.008	0.001	0.007	0.010	1.056
ϕ_S	Phi_S	2.001	1.589	0.549	5.438	1.018
θ_S	$Theta_S$	0.779	0.230	0.494	1.198	1.018
δ_S	$Delta_S$	0.636	0.295	0.160	1.141	1.033
σ_S	$Sigma_S$	1.039	0.204	0.746	1.400	1.029
ζ	$Zeta$	8.470	5.391	2.632	20.421	1.012
$\psi_{1,G}$	$Psi_{1,G}$	-0.178	0.842	-1.768	0.977	1.010
$\psi_{1,F}$	$Psi_{1,F}$	-1.080	0.681	-2.295	-0.042	1.006
ψ_2	Psi_2	1.655	0.723	0.489	2.850	1.011
$\bar{\gamma}_{H0}$	$Gamma_{H0}$	6.137	0.095	5.979	6.293	1.085
$\bar{\gamma}_{HA}$	$Gamma_{HA}$	3.970	0.098	3.811	4.130	1.091
σ_H	$Sigma_H$	0.726	0.050	0.648	0.810	1.058
τ	Tau	146.806	14.597	124.830	172.699	1.061
ν	Nu	0.289	0.502	0.001	1.468	1.054
η	Eta	0.043	0.014	0.022	0.068	1.010

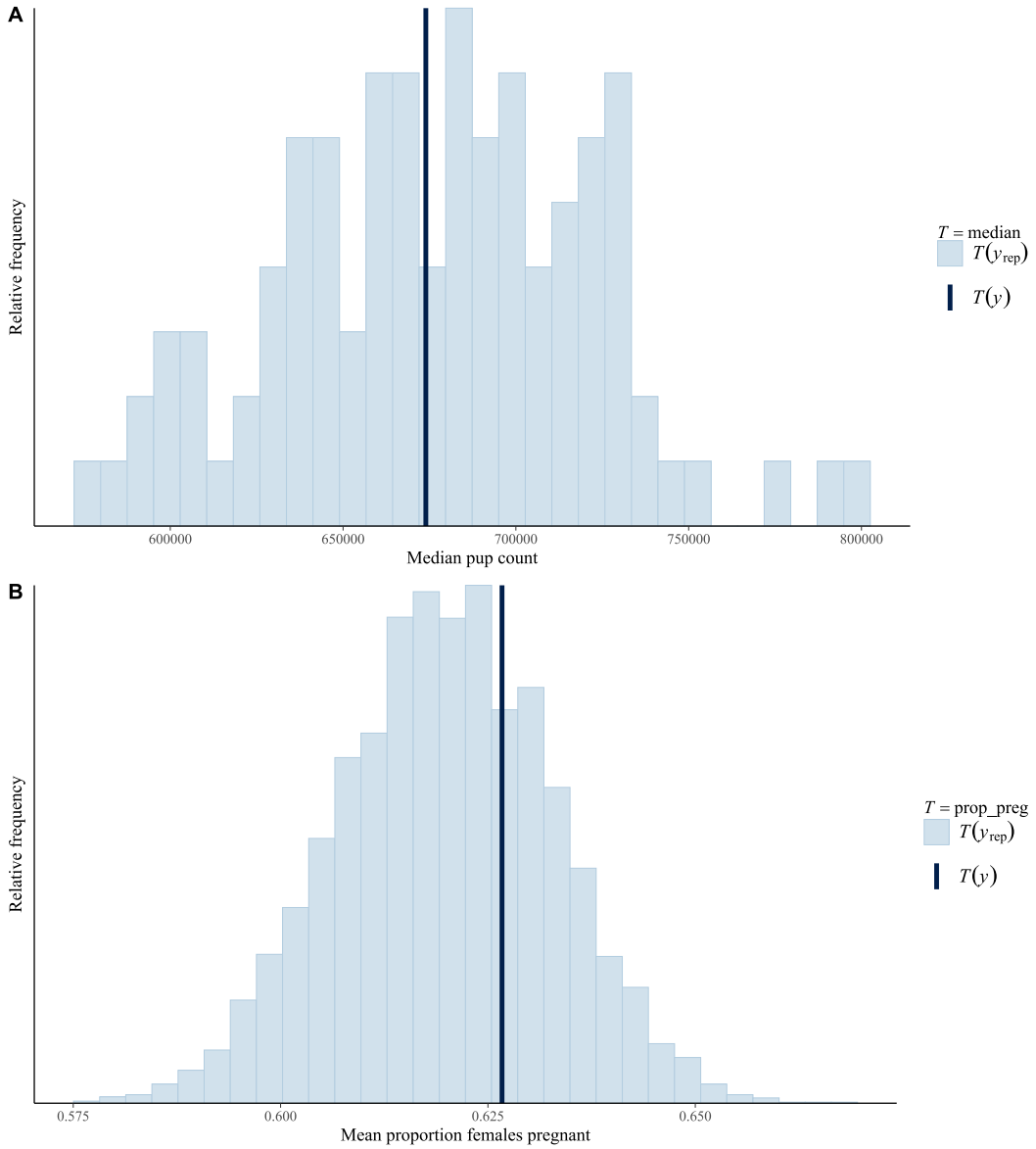

Figure 7. Graphical representation of posterior predictive check (PPC) diagnostics. A) median pup counts based on observed data (black line, "y") compared to histogram of replicate out-of-sample or "new" observations (light grey bars, "yrep") generated by the model. B) median proportion of females pregnant (black vertical line, "T(y)") compared to a histogram of equivalent mean values for replicate out-of-sample or "new" observations (light grey bars, "T(yrep)"). In both plots the distribution of out-of-sample observations, drawn from the relevant probability distributions, are consistent with observed values, indicating a good fit of the model.

Fecundity rates varied as a function of age for females older than 3 years (females aged 3 and younger rarely produce viable pups), increasing rapidly and reaching an asymptotic value by age 8 years. Fecundity rates also decreased as population abundance increased (Figure 8).

As with fecundity, survival rates varied as a function of age, with first year survival (S_0) substantially lower than adult survival (S_A), especially at higher densities (Figure 8). Density-dependent variation in survival is negligible for adults but substantial for juveniles, with an accelerating decrease in survival as abundance increases above 6 million animals (Figure 9).

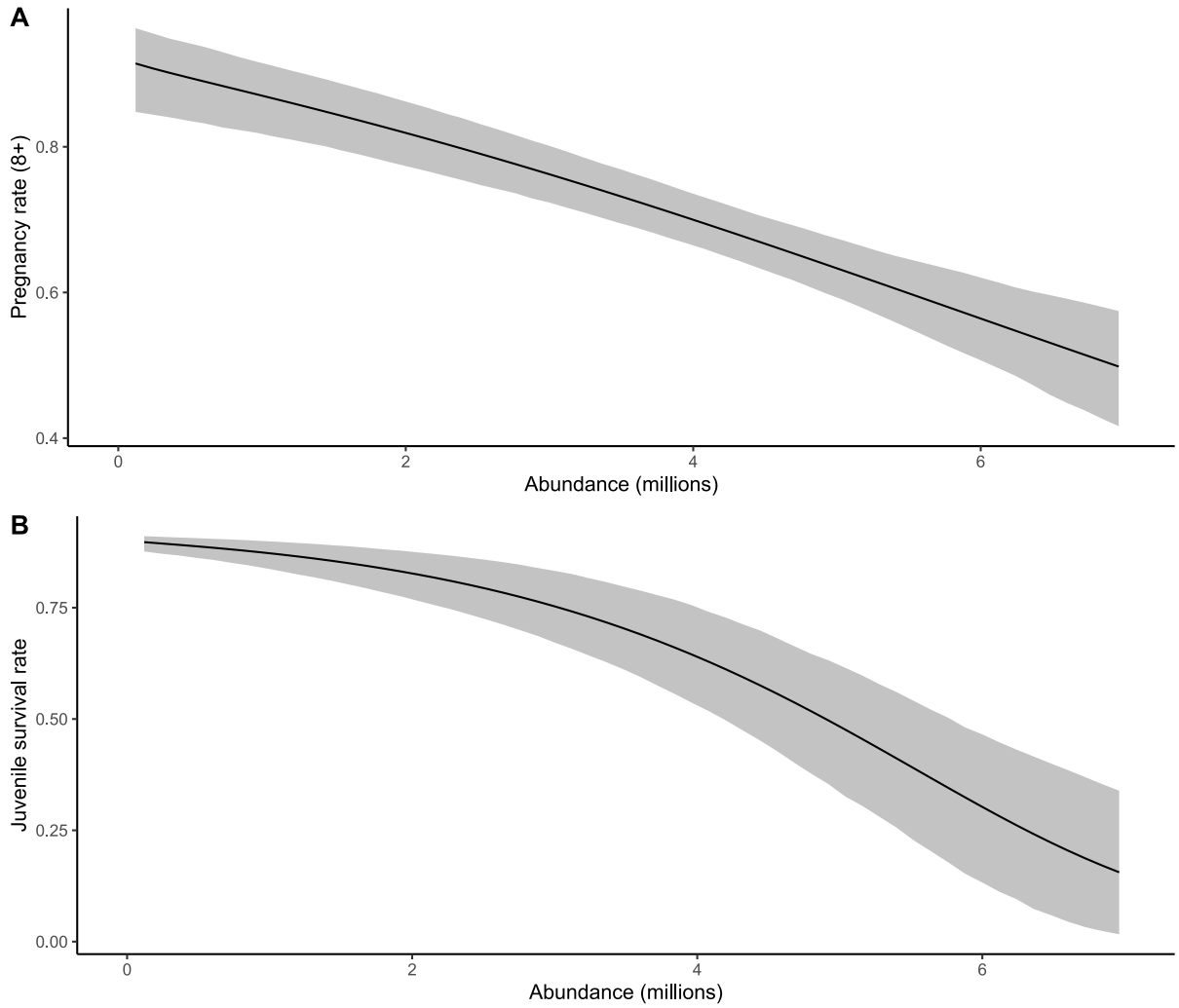

Figure 8. Plots showing relationship between model-estimated vital rates and population abundance: A) adult female fecundity (proportion of females aged ≥8 years that are pregnant), and B) annual survival rate for juveniles (young of the year). Solid lines indicate mean estimated values and shaded bands indicate the associated 95% CI.

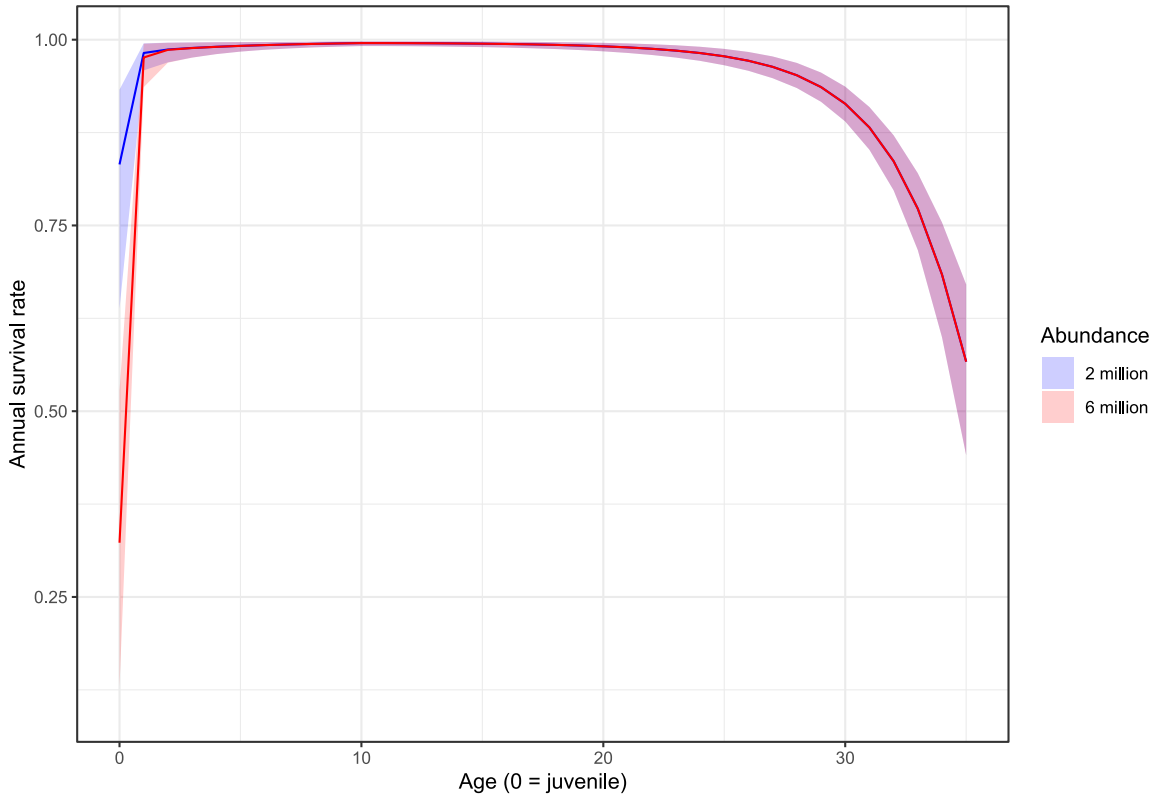

Figure 9. Plot of model-estimated relationship between annual survival rates and age: solid lines indicate mean estimated values and shaded bands indicate the associated 95% CI. The age-specific survival curves are plotted for two population densities to illustrate density-dependent effects.

The Newfoundland Climate Index (NCI) had a significant negative effect on fecundity, accounting for some of the variation in pregnancy rates (Figure 10). After accounting for these fixed effects, environmental stochasticity resulted in substantial deviations from mean expected fecundity rates over time, with occasional “extreme” deviations such as those that occurred in 2010-11 (Figure 11).

The NCI also had significant negative effects on juvenile survival (Figure 10). Years with anomalously low ice cover in both the Gulf of St. Lawrence and the Front (e.g., downward spikes in Figure 4) were associated with reduced pup survival (Figure 12), although this relationship was dampened because the ice-survival relationship was already captured by the effects of NCI (for which ice cover was one of the contributing variables). Finally, after accounting for all fixed effects, environmental stochasticity resulted in significant deviations from mean expected hazard rates for juveniles, with a few notable periods of elevated log hazards such as the early 2000s (Figure 11) contributing to extremely low juvenile survival (Figure 11).

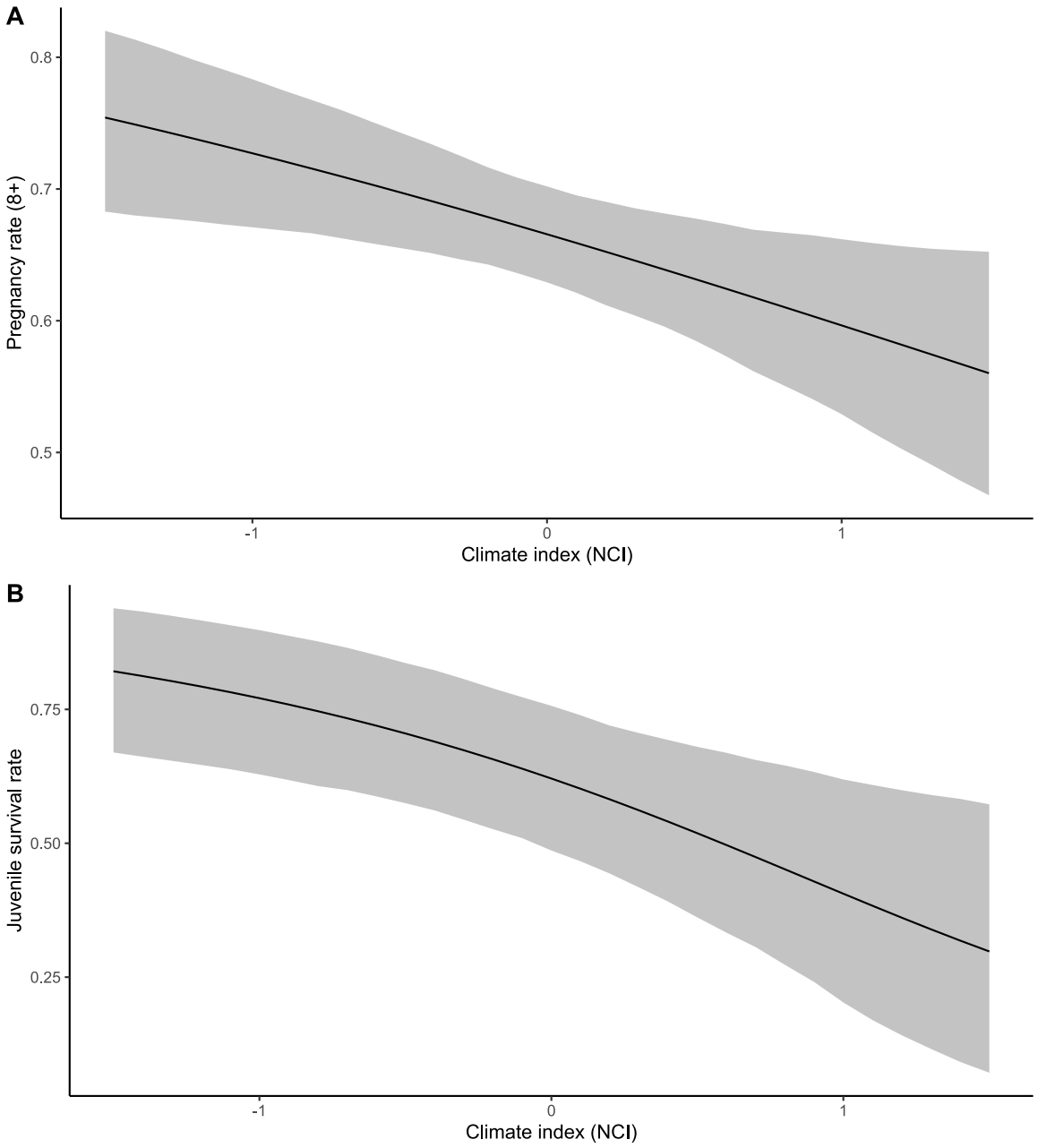

Figure 10. Plots showing relationships between model-estimated vital rates and the Newfoundland Climate Index (NCI). A) adult female fecundity (proportion of females aged ≥8 years that are pregnant), and B) annual survival rate for juveniles (young of the year). Solid lines indicate mean estimated values and shaded bands indicate the associated 95% CI.

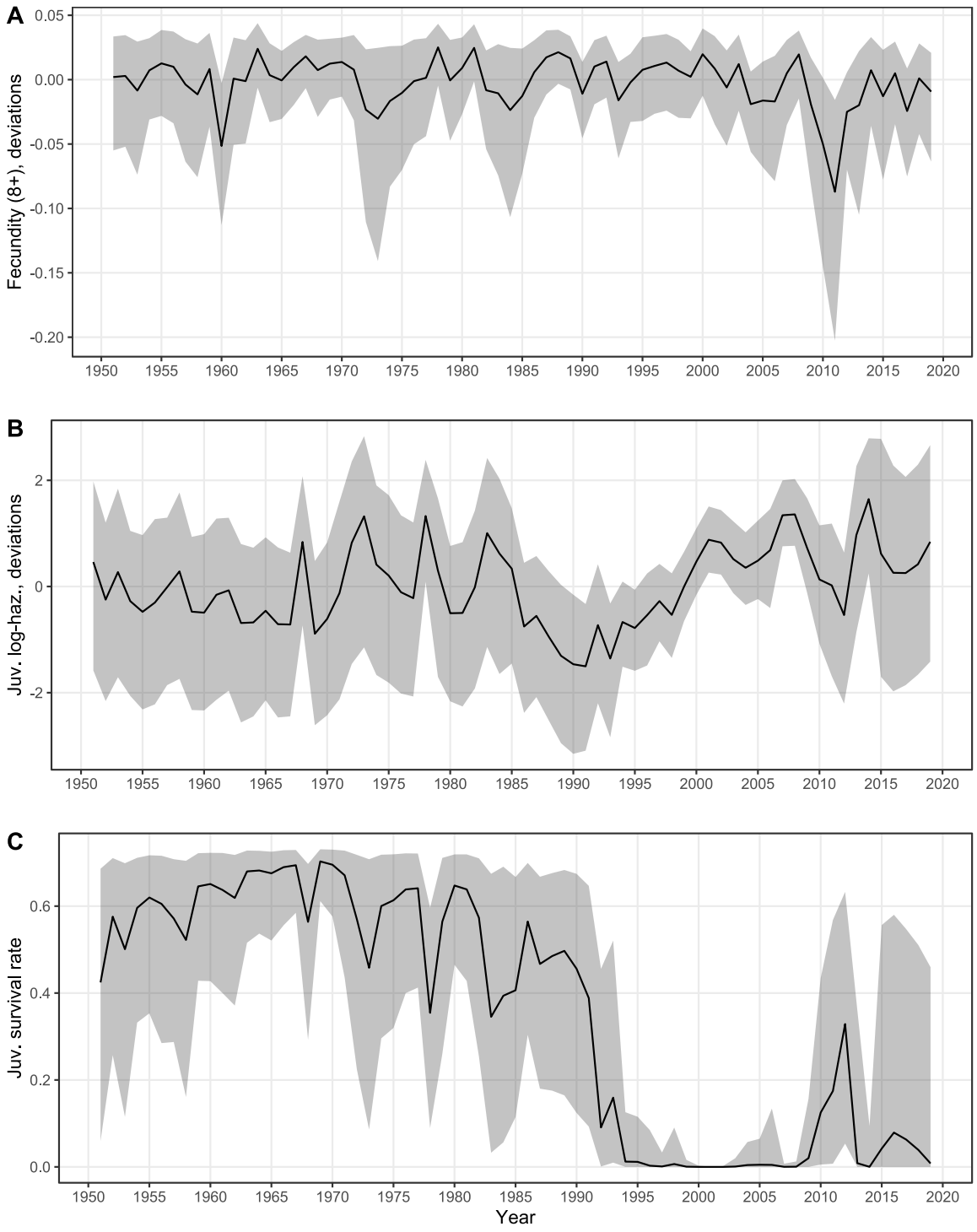

Figure 11. Plots showing stochastic variation over time in model-estimated vital rates: A) deviations from expected adult female fecundity (proportion of females aged ≥8 years that are pregnant); B) deviations from expected log hazard rates for juveniles (young of the year or YOY); C) realized juvenile survival (including stochastic deviations). Solid lines indicate mean estimated values and shaded bands indicate the associated 95% CI.

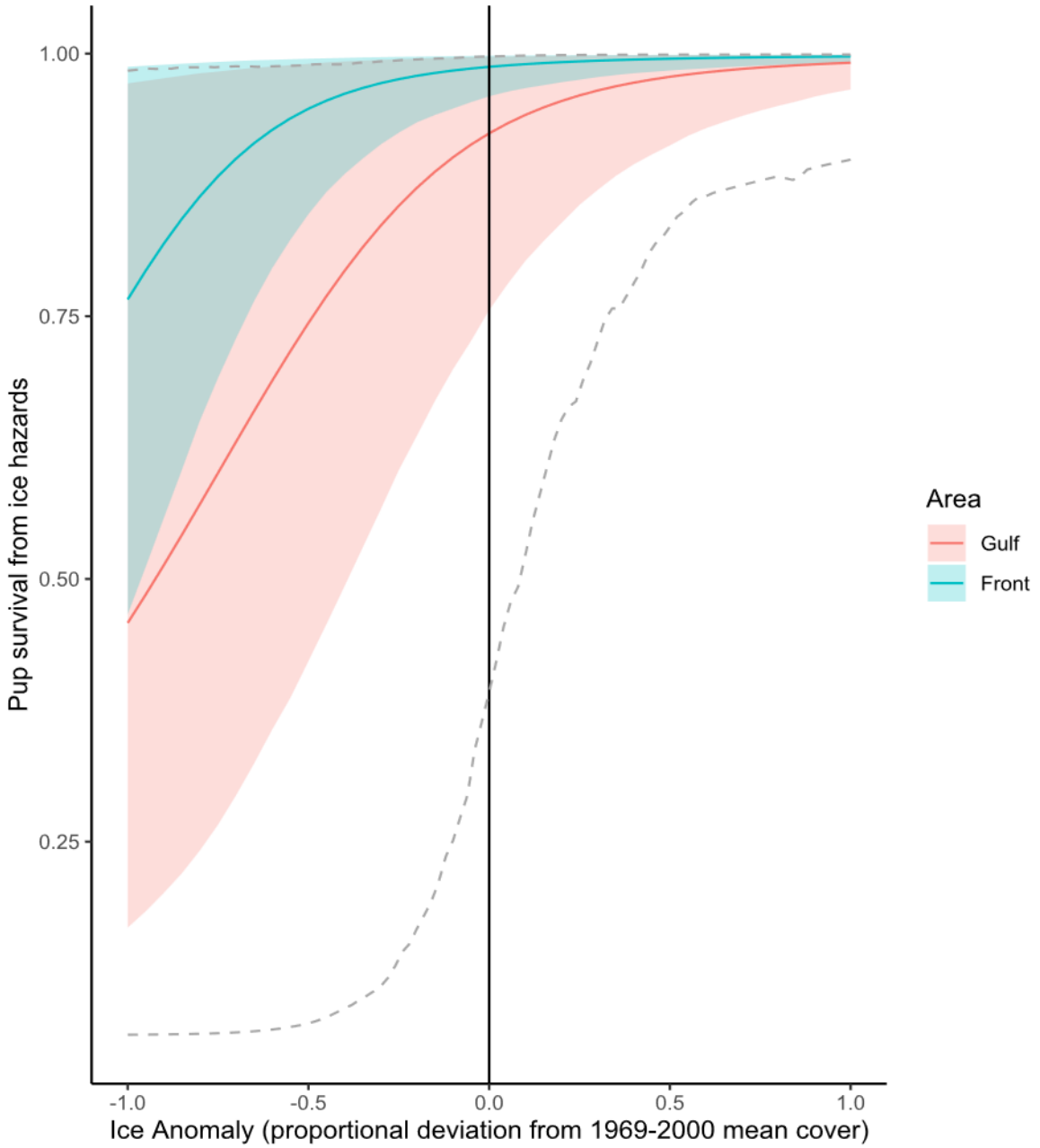

Figure 12. Plot of model-estimated relationships between the ice anomaly index (IC: the proportional deviation from average ice cover values for 1969-2000) and the probability of pup (also known as young of the year or YOY) survival. The effects of IC are estimated separately for the breeding areas in the Gulf of St. Lawrence and the Front. Solid lines indicate mean estimated values and shaded bands indicate the associated 95% CI. Dashed grey lines encompass the 95% quantiles of the prior distribution for the functional relationship, as derived from the priors for the function parameters.

Harvest/bycatch hazards varied substantially over the time series, with the magnitude of variation measured by parameter σ_H (Table 3). Per-capita harvest/bycatch hazard ratios for juveniles (YOY) were >8 times higher on average than equivalent hazard ratios for adults ($\bar{\gamma}_{H0}$ vs. $\bar{\gamma}_{HA}$; Table 3). The estimated temporal variation in annual harvest hazard rates, after

adjusting for struck and loss, were consistent with observed variation in harvest/bycatch numbers (Figure 13).

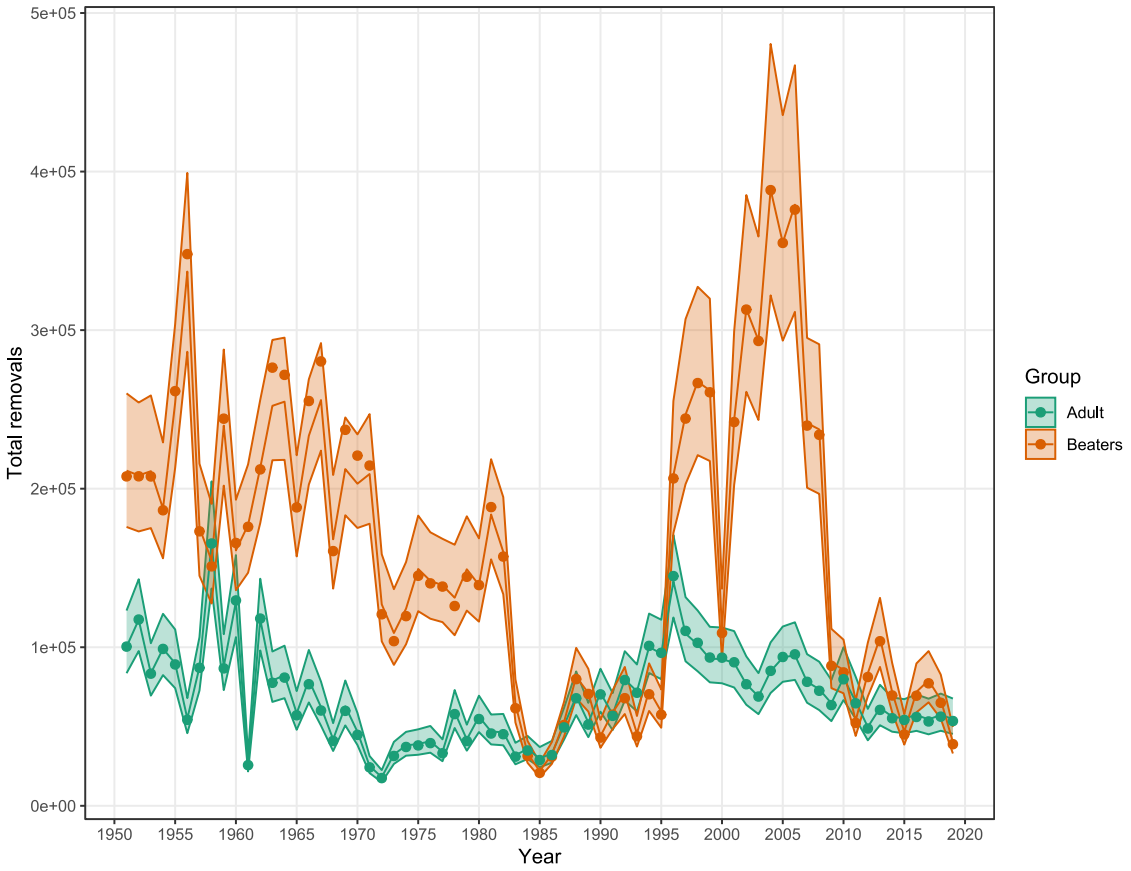

Figure 13. Plot showing temporal variation in model-estimated harvest/bycatch mortality for adults and beaters (also referred to as young of the year (YOY) or juveniles), with observed data plotted for comparison (note that plotted model estimates have been adjusted for struck and loss in order to be comparable to reported deaths). Solid lines indicate mean estimated values and shaded bands indicate the associated 95% CI, assuming a coefficient of variation in reported harvests of 10%.

When all of the estimated environmental and demographic effects, as well as harvest/bycatch mortality, are combined, the model results indicate that human removals represent the single most important driver of juvenile mortality up until 1985. However, since 1985, density dependent mortality and unexplained stochastic deviations have been a more substantial source of juvenile mortality, followed by anthropogenic removals between 1996 and 2006 (Figure 14). Mortality attributable to ice anomalies and climate effects (NCI) are also important in some years, particularly in more recent decades (Figure 14).

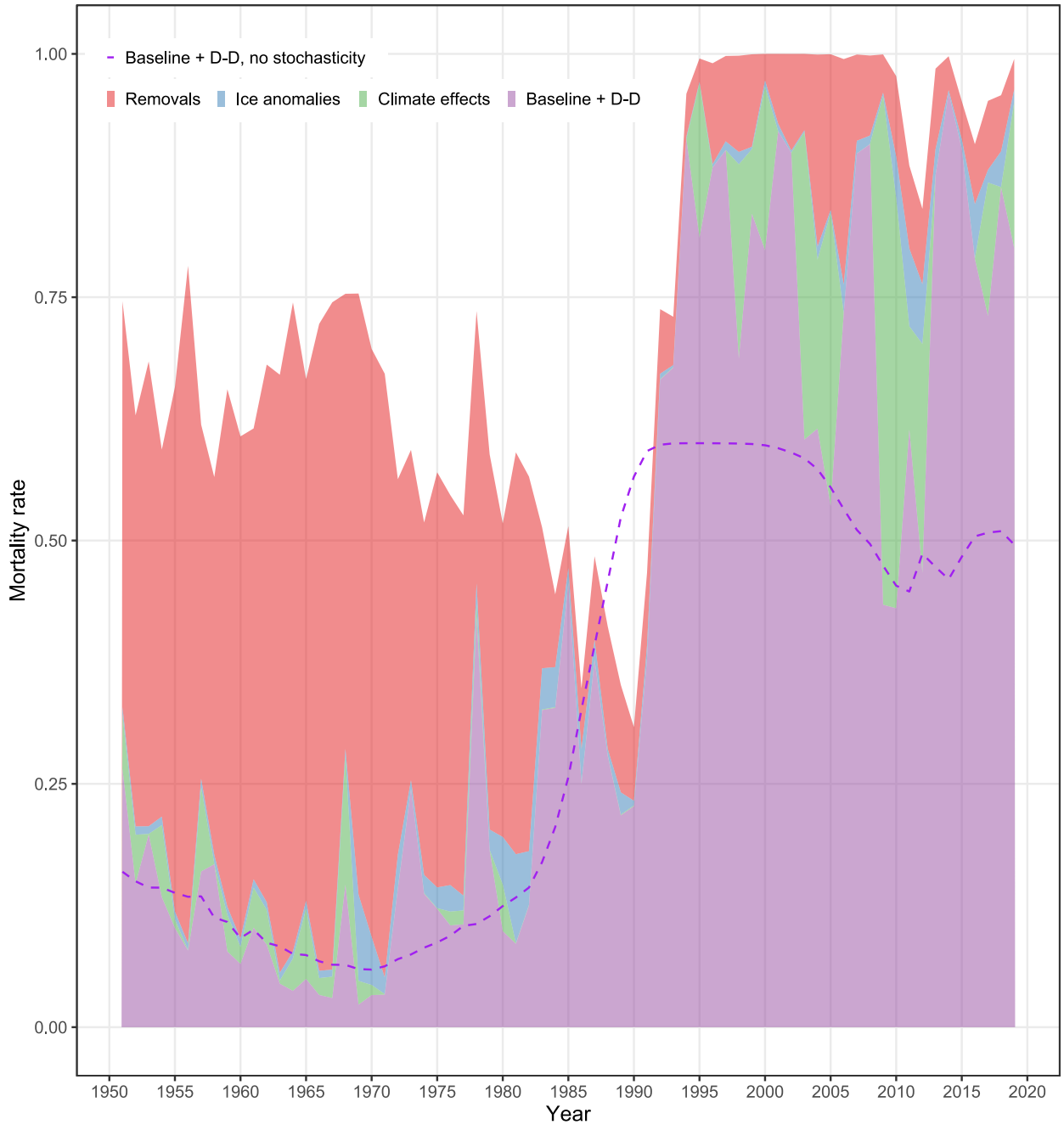

Figure 14. Plot showing relative contributions of various sources of mortality to the total combined mortality rate for juveniles (also referred to as YOY). Mortality factors compared include removals from harvesting (taking into account struck and loss and incidental catches), mortality attributable to poor ice conditions, mortality attributable to climate effects, and baseline plus density-dependent mortality (including stochastic variation). The dashed line indicates what the expected value of baseline plus density-dependent mortality would be if stochastic variation were excluded.

The various sources of mortality and fecundity are combined in the process model to generate projections of population dynamics. Using the Stochastic model, the 2019 estimate of pup production is 776,000 (95% CI 558,000- 1,011,000) and the total estimated abundance is 4,667,000 (95% CI: 3,712,000- 5,679,000). The Stochastic model projections are generally

consistent with observed data sets in terms of temporal variation in adult pregnancy rates (Figure 15), pup counts (Figure 16), and relative age structure (Figure 17). When compared with observed data or equivalent projections from the deterministic model, the Stochastic model projections more closely adhered to variation in the three empirical time series: most observed data points (or their standard error bars) intersected the 95% CI bounds of the Stochastic model projections. In the case of the Deterministic model, the model provided a good fit to the reproductive data, in cases where sample size was greater than or equal to 40, which represented most years after 2000, but the fit to the pup production estimates and ability to track changes in age structure was not as good, particularly during the latter two decades (Figures 16-17).

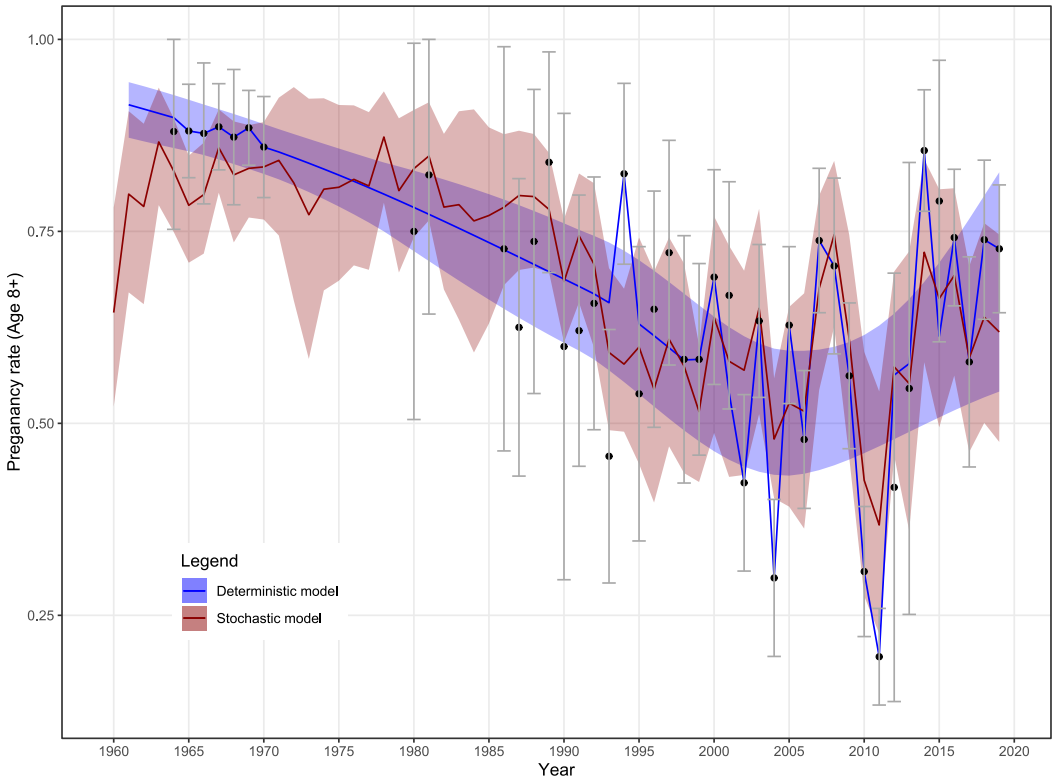

Figure 15. Plot showing temporal variation in model-estimated pregnancy rates (for females ≥ 8 years) with observed data plotted for comparison: points indicate the mean proportion of sampled 8+ females each year that were pregnant, while error bars show 95% CI associated with the mean observed value based on the variance of a binomial sample. Model projections are plotted for the Stochastic Bayesian model (red) and the data used in the 2019 deterministic model (blue). The Deterministic model used the actual data when samples sizes were 40 or more and the smoothed value in years when samples sizes were less than 40 animals (Hammill et al. 2021). The shaded bands indicate the associated 95% CI that are generated by the stochastic model (red) and the non-parametric smoother in the deterministic model (blue).

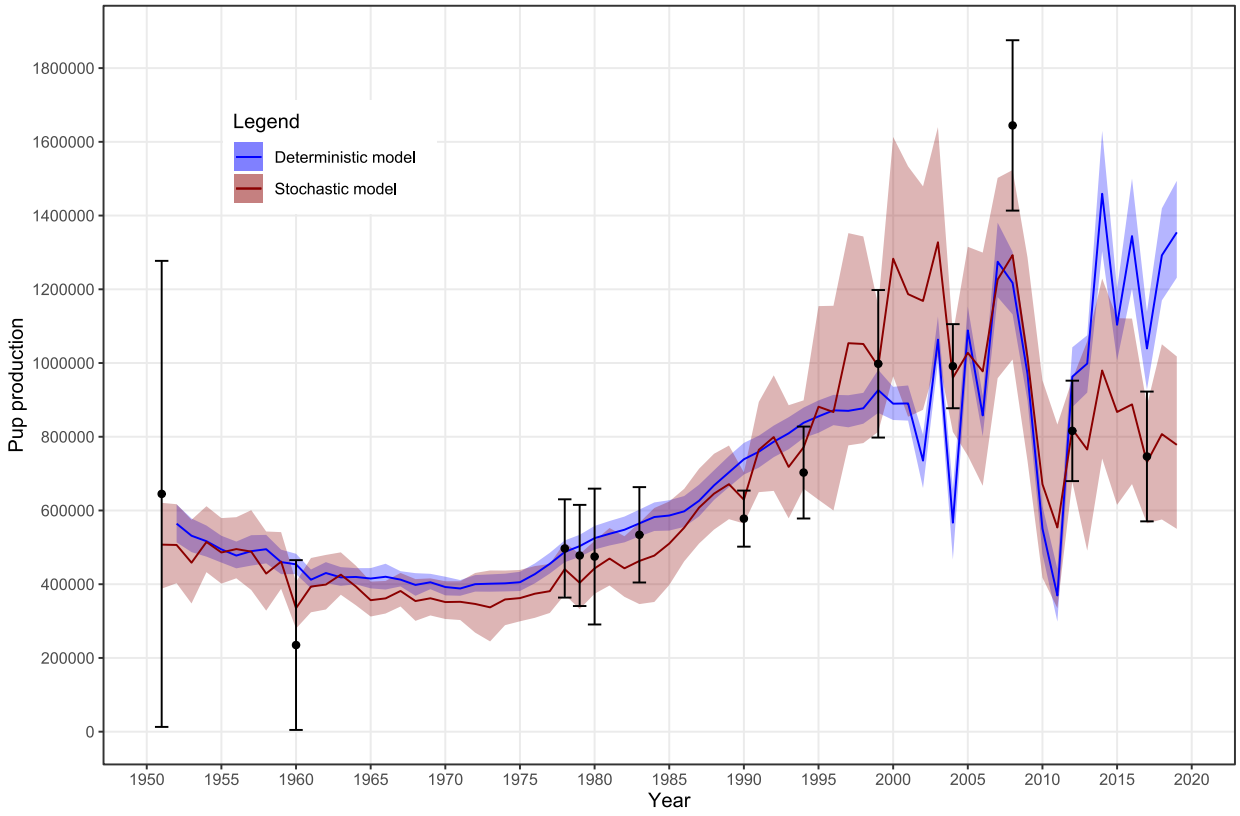

Figure 16. Plot showing temporal variation in model-estimated pup (YOY) production with observed data plotted for comparison: points indicate mean estimated pup abundance for a given survey; error bars show 95% CI associated with the survey estimate. Model projections are plotted for the Stochastic Bayesian model (red) and the Deterministic model (blue). Solid lines represent mean estimated values; shaded bands indicate the associated 95% CI.

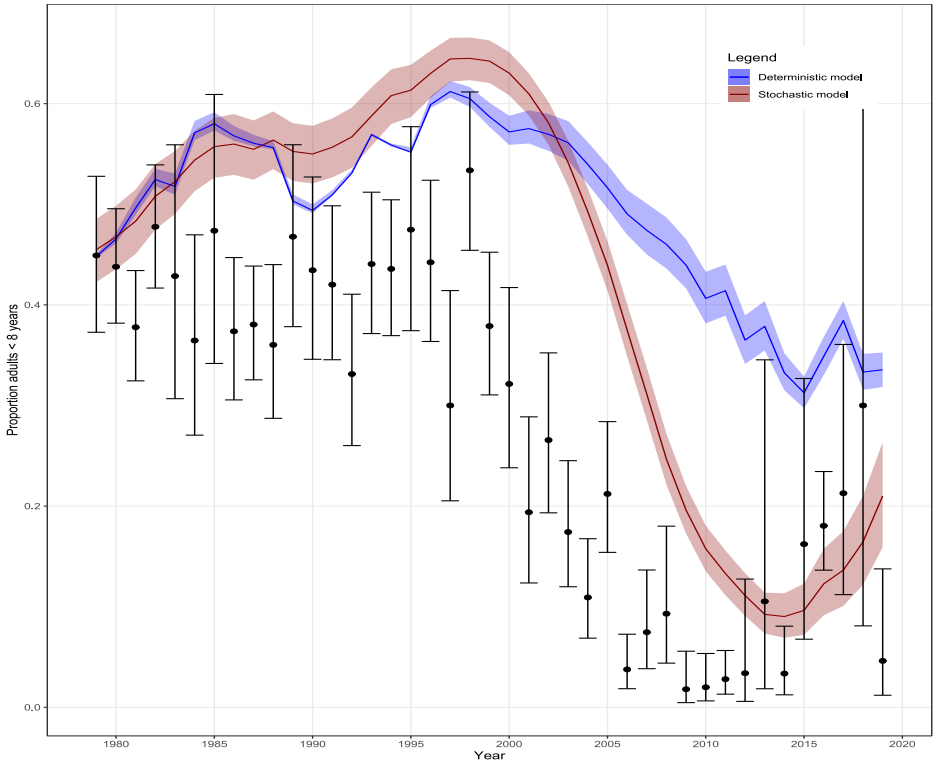

Figure 17. Plot showing temporal variation in model-estimated age structure considering specifically the proportion of animals 5-7 years old versus all animals 8 years old and older. Points indicate the mean proportion based on observation data, and error bars show 95% CI associated with the sampled proportion (based on variance of a binomial sample). Model projections are plotted for the Stochastic Bayesian model (red) and the Deterministic model (blue), with solid lines showing the mean estimated values and shaded band indicating the associated 95% CI.

Total abundance is estimated by the model as a latent variable, although there are no empirical data to compare with. The estimated trends in population abundance (adults plus YOY) based on the Stochastic Bayesian model are shown in Figure 18, with corresponding estimates from the Deterministic model shown for comparison. The two models are generally consistent in their projections from 1951 through approximately 1990 but deviate after that point. The Deterministic model projected a relatively flat trend from 1995 – 2010, followed by a small decline from 2009 – 2011, then a substantial increase from 2012 – 2019 to a historic high abundance of over 7 million. In contrast, the Stochastic model indicates a stronger increasing trend between 1990-1997 to a high of 6.6 million, followed by a substantial decline between 2000 – 2011 to 4.2 million, and then a modest increase from 2012 – 2019 to 4.7 million. Despite these differences, it is notable that the uncertainty intervals of the two model projections overlap each other for much of the time series with the exception of 1950-58, and since 2015 (Figure 18).

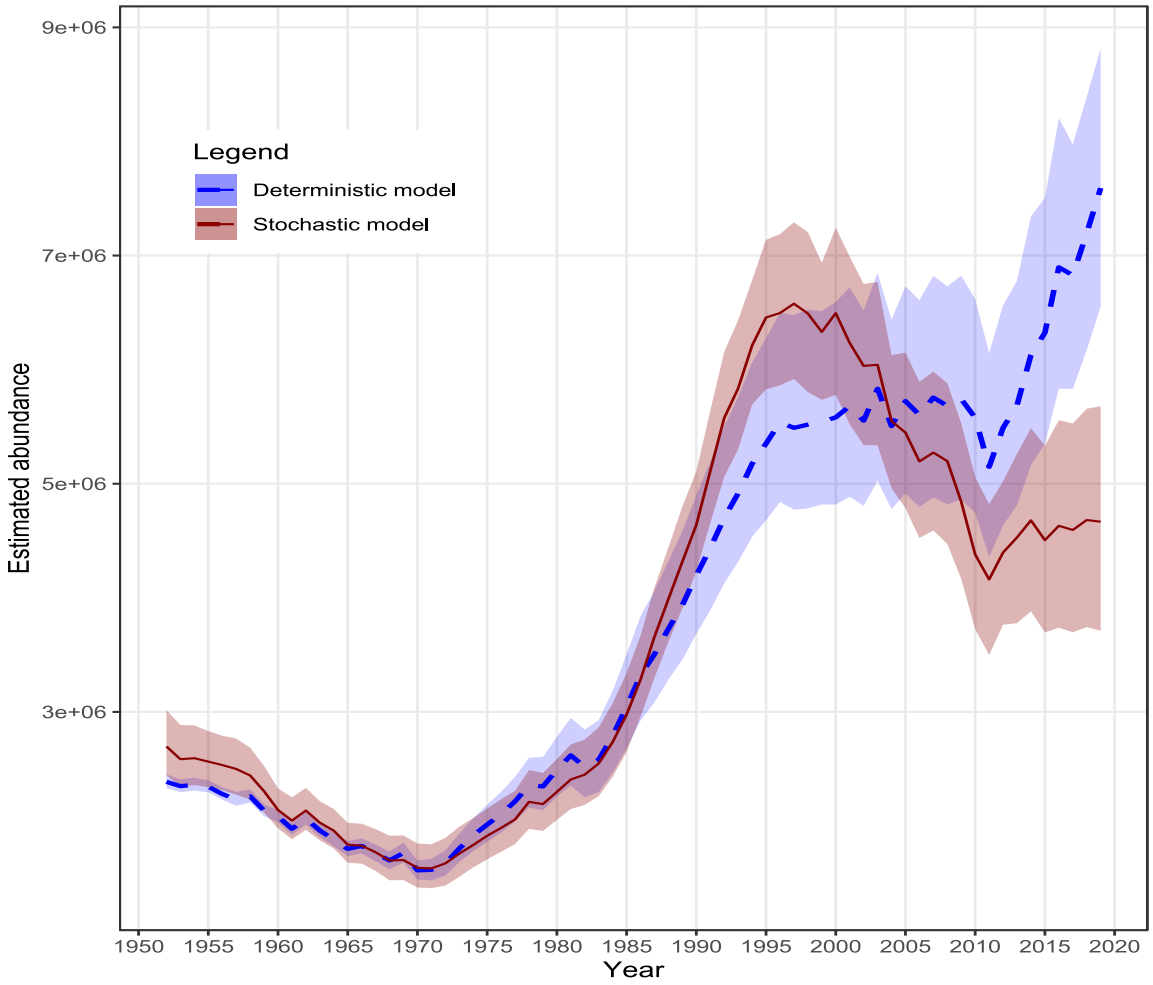

Figure 18. Plot showing temporal variation in model-estimated abundance for the Stochastic Bayesian model, with a start age of 5 years (red) and the deterministic model (blue). Solid and dashed lines represent mean estimated values for the Stochastic and Deterministic models, respectively, while shaded bands indicate the associated 95% CI.

As an additional posterior predictive check of the Stochastic model goodness-of-fit, we used Monte Carlo methods to generate “out-of-sample” hind-cast projections of population dynamics (initiated with the estimated abundance in 1951 and projected forward with random effects not fit to the data). The distribution of hind-cast, out-of-sample projections encompasses the actual model estimated trends in population abundance, further supporting the goodness of fit of the Stochastic model (Figure 19). However, it is worth noting that since approximately 2006 the fitted model trend falls near the lower 95% quantile of the distribution of hindcast simulations, reflecting the fact that stochastic deviations in juvenile mortality were consistently elevated over this period (Figure 11). This suggests a persistent shift in environmental and/or anthropogenic mortality sources.

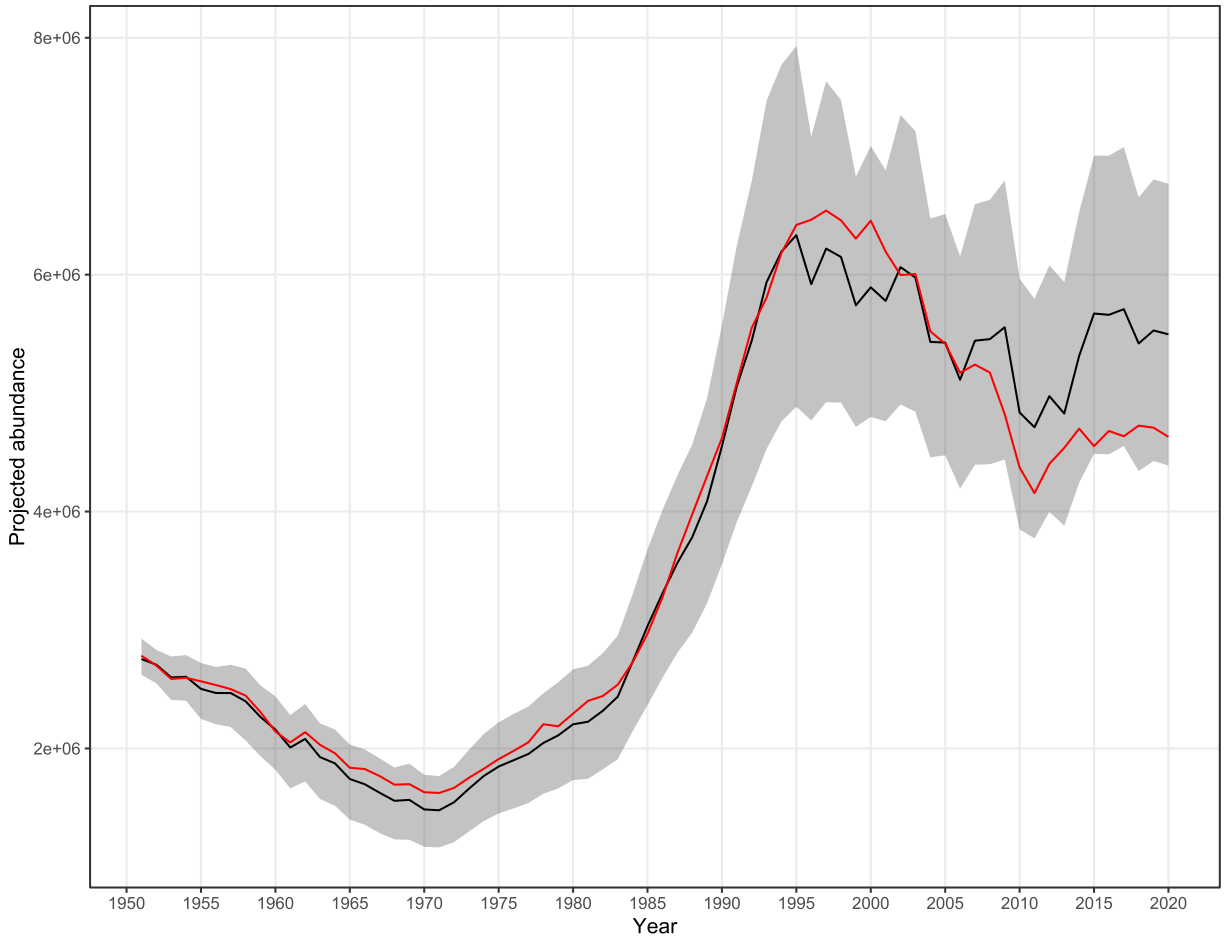

Figure 19. Plot showing the distribution of random hind-cast model projections of harp seal abundance over time (grey shaded band with black line showing mean) compared to the actual model-estimated trends (red line) for a start age of 5 years old. For hind-cast projections, the model was initiated with the estimated 1951 abundance, all parameters were drawn randomly from joint posterior distributions, and the process model was iterated forward with random effects drawn from appropriate sampling distributions but not fit to data. Thus each iterated hind-case simulation represents an "out-of-sample" model projection of a possible population trajectory, given the estimated range of environmental stochasticity. For a well-fit model the estimated trend should fall within the distribution of out-of-sample projections.

To estimate realized carrying-capacity (*K*) in the absence of human-caused mortality, future projections of population dynamics were generated using Monte Carlo simulations of the model (with harvest/bycatch hazards forced to 0) under two scenarios of future ice cover and environmental conditions. The distribution of future projections stabilized after several decades (Figure 20), with the mean long-term abundance for each scenario corresponding to an equilibrium abundance estimate (*K)* in the absence of harvest/bycatch mortality. In the first scenario, climate index and ice cover variables were drawn randomly from their pre-2000 distributions which produced an estimated equilibrium abundance of 7.6 (SD=0.09, 95% CI=7.43-7.76) million harp seals. In a second scenario, climate index and ice cover variables were drawn from their post-2000 distributions to represent current conditions. This resulted in an equilibrium estimate of 6.79 (SD=0.07, 95% CI=6.68-6.91) million harp seals.

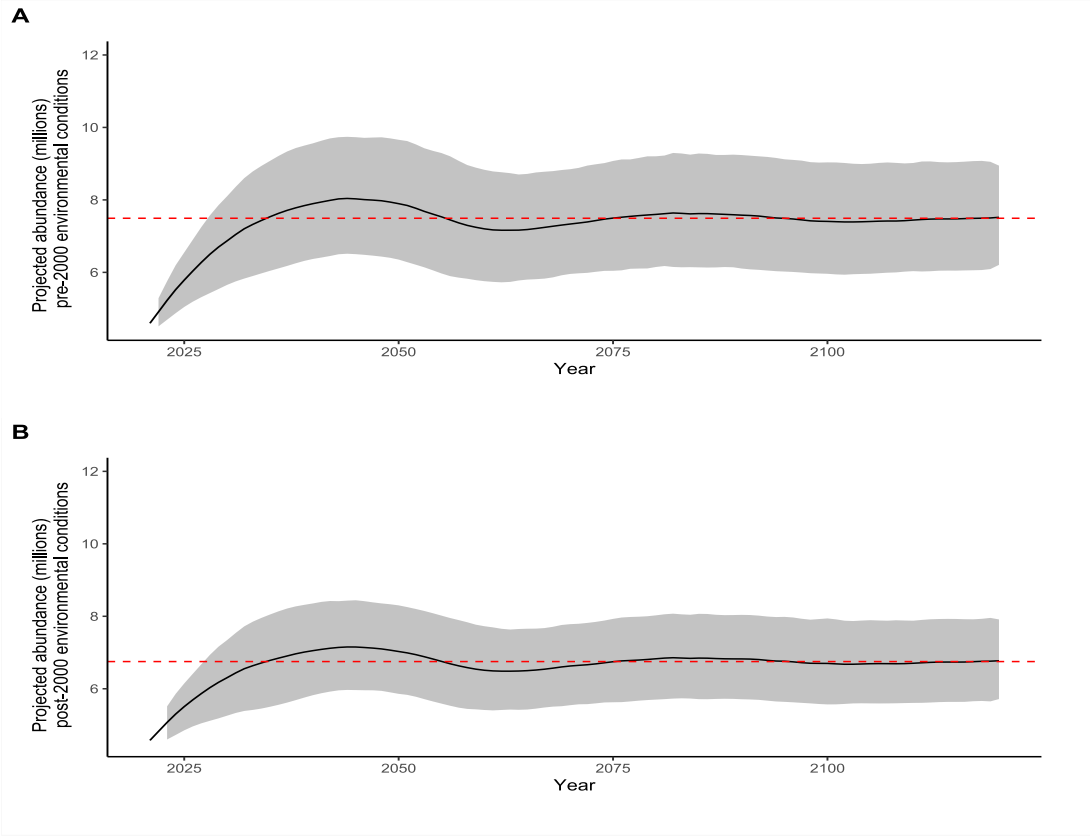

Figure 20. Plots showing future projected abundance of harp seal populations, with harvest/bycatch mortality forced to 0, under two alternative scenarios of ice cover and environmental conditions: A) ice cover anomalies (IC) and Newfoundland Climate Index (NCI) are drawn from the empirical distributions observed over the period 1969 – 1999; and B) IC anomalies and NCI are drawn from the empirical distributions observed over the period 2000 – 2020. For both plots, the red line indicates the mean expected value over the last 50 years of the 100-year projection, and can be interpreted as "K", or the expected equilibrium abundance (for the specified scenario) in the absence of direct human mortality.

DISCUSSION

Previous runs of the Deterministic population model had suggested that abundance declined through the 1950s and 1960s to an estimated minimum of approximately 2 million animals in 1972, before recovering to an estimated 7.6 (95% CI=6.55-8.82) million animals in 2019 (DFO 2020; Hammill et al. 2021). Prior to the 2019 assessment, the Deterministic population model had provided a reasonable fit to the pup abundance and reproductive rate data. However, at the last assessment the model fit was not only poorer, but a marked change in population trend was identified, changing our perception from one of a population that had recovered rapidly since 1982, peaking at 7.4 million animals in 2008 then levelling off at just over 7 million animals, to one of a population that recovered rapidly since 1982, had levelled off at approximately 5.5 million animals in 1996 and after a slight dip in 2011, had showed renewed growth in the absence of high harvests, increasing to 7.6 million animals by 2019 (Hammill et al. 2015, 2021). Hammill and Stenson (2009) concluded that a deterioration in the model fit to the survey data pointed to underlying problems relating to model assumptions and or structure, such as failure to consider ice-related mortality and its impact on juveniles. Incorporating ice-related mortality into the assessment model improved the fit somewhat, until recently. In the 2019 assessment, however, the poor fit of the assessment model to the 1990, 1994, 2008 and 2017 aerial survey

estimates further indicated that the Deterministic model was unable to capture the full range of dynamics present in the available data sets.

The Stochastic model presented here shares many features with the previous Deterministic model, in that the process model tracks fecundity, survival, and abundance of multiple (36 in stochastic, 27 in deterministic) year classes. To aid in comparing the two models, we used (to the greatest extent possible) the same input data as presented in Hammill et al. (2021). However, there are several important ways in which the Stochastic model structure differs from the Deterministic model, summarized in Table 4. The key difference is the relaxation of the assumption that demographic processes are fixed (deterministic) and the allowance for environmental stochasticity in vital rates, which is achieved by fitting the process model to observed data within a hierarchical Bayesian framework. A key advantage of the Bayesian approach is the ability to combine multiple sources of data and fully characterize uncertainty within a single, integrated modelling framework (Brandon and Wade 2006). The hierarchical framework can allow for estimation of missing states as well as the sharing of information across data sets or surveys, which can improve estimation and increase precision (Sigourney et al. 2021). Moreover, the use of prior information can be included in a formalized manner when direct information is lacking. Another important difference was that the Stochastic model incorporated age-structure information from the Newfoundland sampling program into the fitting process. The inclusion of age structure data greatly improved the power to estimate variation in age-specific survival rates.

Table 4. Comparison of the features and attributes of two models used to estimate NW Atlantic harp seal abundance and population dynamics: the Stochastic, Bayesian hierarchical model and the previous deterministic model. The term "model-fit" refers to parameters estimated by fitting to data, "fixed" refers to parameters set by the user (i.e., based on expert opinion or on previously published information). Acronyms used: "fxn" = "function"; "D-D" = "density dependent"; PHF = "Proportional Hazards Function"; "M-Ice" = excess mortality associated with ice cover anomalies.

Feature/Attribute	Bayesian hierarchical Stochastic model	Deterministic model
Data sets		
Pup counts	Used for fitting, assume gamma distribution	Used for fitting, assume normal distribution
Female pregnancy rates (fecundity)	Used for fitting, assume beta-binomial distribution with age covariate (use raw data for fitting)	Used for fitting, when N>40, but "smoothed" prior to model fit if samples <40; assume binomial distribution
Harvest data	Used for fitting, assume normal distribution (accounts for measurement uncertainty and struck and loss)	Not used for fitting, but included as constants for calculations of annual population dynamics
Age structure data (adults)	Used for fitting (for survival schedule), assume Dirichlet-multinomial distribution to account for over-dispersion/variance	Not used as input
Ice cover	Annual anomalies in ice cover of the Gulf and Southern Labrador from Canadian Ice Service used as covariate of juvenile mortality: effect estimated as a continuous hazards function	Annual anomalies in ice cover of the Gulf and Southern Labrador from Canadian Ice Service used as covariate of juvenile mortality: effect assumed, not estimated, with-adhoc setting of mortality threshold
Process Model		
Fecundity function	Model-fit: non-linear, 2-parameter logit fxn for age, assumed to asymptote after 8yrs, also includes D-D (2 parameter theta-logistic fxn) and environmental stochasticity terms (hierarchical random effect)	Fixed max rate for 8+, D-D is model-fit using 2 parameter theta-logistic fxn (theta parameter fixed). Environmental effects on K fixed. No stochasticity. Age differences allowed using Gaussian copula
Mortality, Juvenile	Model-fit, incorporates competing hazards using PHF (baseline, D-D, M-Ice, harvest), allows for env. stochasticity. Non-linear D-D and M-ice functions are also model-fit (D-D pars independent from fecundity). Competing hazards from harvest treated as model-fit, time-varying hierarchical parameters.	Mortality of adults or juveniles fixed, or juvenile mortality fixed as a multiplier of adult mortality which was estimated in earlier models. In 2019 adult mortality fixed and juvenile mortality was estimated and. Allows for M-Ice, but relationship between M-Ice and ice cover is assumed/fixed, not fit. Allows for D-D, but D-D function is same as Fecundity D-D function (i.e., same "K" parameter, fixed theta). Additional mortality from reported harvest incorporated deterministically

Feature/Attribute	Bayesian hierarchical Stochastic model	Deterministic model
Mortality, Adult (1+)	Model-fit; age variation allowed using 2-parameter, non-linear PHF, with competing hazards from harvest treated as model-fit, time-varying hierarchical parameters	Model-fit in earlier models, fixed in most recent model; no age-variation. Additional mortality from reported harvest incorporated deterministically
Initial abundance	Model-fit; initial age structure set as the stationary distribution associated with estimated vital rates	Model-fit; initial age structure assumed
Annual dynamics	Standard age-structured transitions, 36 age classes tracked, survival varies by age	Standard age-structured transitions, 27 age-classes (survival constant across 1+ ages). Age classes not tracked
Model fitting		
Method	Bayesian MCMC: all parameters estimated as joint posteriors fit to all 4 data sets (pup counts, pregnancy rates, harvest data and age structure) with appropriate distributions for each. Vague priors for all params except ice mortality function parameters (for which moderately-informed priors)	“Pseudo-likelihood”: brute-force sims used to find minimum combined sum of squared Pearson residuals for pup counts and pregnancy rates (for 8+ females). This assumes both observed variables are normally distributed, but no formal variance weighting.
Evaluation	Ensure model convergence and mixing of independent chains, posterior predictive checks and goodness of fit diagnostics. Visually evaluate agreement between predicted trends and raw data sets	Visually evaluate agreement between predicted trends and raw data sets

Because the samples used to determine age structure of the population were collected for a variety of reasons, it is possible that some age groups, particularly younger seals, may have been over or under estimated. However, the younger age classes are most likely to be impacted first by changes in density-dependent or environmental conditions (e.g. as per Eberhardt 2002) and so, excluding these younger animals in model fitting may affect our ability to detect changes in demographic rates, introducing additional lags between when significant demographic changes might occur and when they can be fully incorporated into the population model. The utilization of information theory and model comparisons via LooIC allowed for alternative versions of the model (with differing minimum age) to be assessed objectively in terms of the relative degree of support (see Appendix 3). This approach suggested more support for a minimum age of 5 years old to be included in age structure data used for model fitting. Further evaluating the impact of including younger age classes on model estimates is one area that could be investigated further.

Climate change is expected to have a negative impact on harp seals through loss of ice for breeding and likely through impacts on food resources (Stenson et al. 2020b). The Stochastic model uses a proportional hazards formulation to model survival, which provides a mathematically coherent way to incorporate and estimate multiple competing sources of mortality (hazards). Using this approach, uncertainty in reported catches, ice cover during the pupping season and an environmental index (Cyr and Galbraith 2021) were identified as factors affecting juvenile survival. Differences in mean ice cover in the Gulf and at the Front during peak pupping were used to build the ice anomaly index. This index provides insights into conditions

when the pups are born, but harp seal YOY require a stable ice platform for a period of 4-6 weeks after birth. Unfortunately, this index as currently calculated is unable to capture changes in ice cover due to storms, or early breakup, after pupping has occurred, which likely limits its sensitivity as a predictive variable for pup survival. The more generalized Newfoundland Climate Index (NCI) incorporates information on water and air temperatures, windspeeds and total accumulated ice cover in Atlantic Canada over the entire year. Because the NCI incorporates ice cover variables, there is some degree of overlap and co-linearity between the NCI and the ice anomaly index. The two indices are still somewhat distinct: for example, the ice-anomaly represents conditions at peak pupping, whereas the NCI includes total accumulated ice over the season, and ice cover is only one of many variables contributing to the composite NCI, which reflects general environmental (oceanographic) conditions in the Northwest Atlantic (Cyr and Galbraith 2021). However, in our fitted Bayesian model the estimated NCI effects on survival and pregnancy rate were quite strong, whereas the estimated effects of ice-anomaly were weaker, suggesting that the NCI effects might be accounting for much of the mortality that would otherwise have been attributable to ice anomalies. Further work is needed to better quantify changes in the quality of the ice platform during the 6 week period critical for YOY, as well as understanding the contribution of other environmental factors to juvenile survival. The use of proportional hazards provides a useful framework allowing for these questions to be explored.

The Stochastic model provided a 2019 pup production estimate of 776 thousand and a total abundance estimate of 4.7 million, which is approximately 62% of the estimated 2019 total abundance of 7.6 million produced by the Deterministic model (Hammill et al. 2021). The higher estimate from the Deterministic model reflects multiple differences in the two models (Table 4), perhaps most importantly the limiting assumption of the Deterministic model that juvenile mortality is fixed over the entire time series, and thus unexplained increases in mortality (such as those that have occurred since 2000; Figure 11B) cannot be captured. Once harvesting declined, the fixed mortality rate of the deterministic model inevitably assumed an increase in population abundance. In the Stochastic model, juvenile mortality from density-dependent and density-independent factors (including poor ice conditions and climate forcing) were not assumed to be fixed, and thus captured the effects of increased mortality after 2000. In the absence of high harvests, these sources of natural mortality are (and likely will continue to be) the major factors driving the dynamics of this population (Figure 14). Recent assessments of grey seals also resulted in downward revisions to estimates of total abundance of a similar order of magnitude due to significant changes in how juvenile mortality is incorporated into assessment models. Both of these cases highlight the importance of improving our understanding of this key parameter (Rossi et al. 2021).

Another important advantage of the integrated Stochastic Bayesian model is the ease with which the fitted process model can be adapted for generating forward projections of population dynamics, accounting for parameter uncertainty (by drawing from the joint posterior distribution of all parameters) and using appropriate distributions of random effects. We took advantage of this feature to explore the potential equilibrium abundance (K) in the absence of harvest mortality, under differing assumptions about future variation in environmental conditions (i.e., ice anomalies and NCI index). Comparing the results of future simulations under temporal distributions of environmental variables corresponding to pre-2000 conditions, vs. post-2000 conditions, shows compellingly that the effective K for harp seals has decreased over recent decades, with an equilibrium abundance approximately 1 million seals lower than was expected under pre-2000 conditions. As environmental and ice conditions deteriorate, K is also expected to continue to decline, affecting juvenile survival first, unless harp seals are able to adapt by finding suitable environmental and ice conditions further north.

In summary, the Stochastic model improves upon the Deterministic model in several ways, including: 1) variables that were treated as fixed constants in the Deterministic model are now treated as estimated parameters in the Stochastic model, allowing for data-driven estimates of annual age-specific survival, density-dependent effects, mortality from ice anomalies, and effects of environmental conditions on fecundity and survival; 2) the Stochastic model allows for environmental stochasticity in fecundity and survival; 3) multiple causes of death - baseline mortality, age and density-dependent effects, pup mortality due to poor ice cover, harvest/bycatch mortality - are incorporated as competing risks using a proportional hazards formulation, allowing for a more consistent and mathematically coherent treatment of these effects; and 4) model fitting is conducted using a hierarchical Bayesian state-space approach that allows for more robust characterization of uncertainty, disentanglement of process error from observer error, and incorporation of multiple data sources with different distributions and variance structures (Buckland et al. 2004, Wang 2009, Williams et al. 2017). Use of the Stochastic model for future assessments, and for exploring potential consequences of a changing climate, will help strengthen and support management of this iconic species.

REFERENCES CITED

Brandon, J.R., and Wade, P. 2006. Assessment of the Bering-Chukchi-Beaufort Seas stock of bowhead whales using Bayesian model averaging. J. Cetacean Res. Manage. 8:225-239.

Beyersmann, J., Latouche, A., Buchholz, A., and Schumacher, M. 2009. Simulating competing risks data in survival analysis. Stat. Med. 28:956–971.

Bowen, W.D., and Sergeant, D.E. 1983. Mark-recapture estimates of harp seal pup (*Phoca groenlandica*) production in the northwest Atlantic. Can. J. Fish. Aquat. Sci. 40:728-742.

Bowen, W.D., Capstick, C.K., and Sergeant, D.E. 1981. Temporal changes in the reproductive potential of female harp seal, *Pagophilus groenlandicus*. Can. J. Fish. Aquat. Sci. 38: 495–503.

Brodie, J., Johnson, H., Mitchell, M., Zager, P., Proffitt, K., Hebblewhite, M., Kauffman, M., Johnson, B., Bissonette, J., and Bishop, C. 2013. Relative influence of human harvest, carnivores, and weather on adult female elk survival across western North America. J. Appl. Ecol. 50:295–305.

Buckland, S., Newman, K., Thomas, L., and Koesters, N. 2004. State-space models for the dynamics of wild animal populations. Ecol. Model. 171:157–175.

Carpenter, B., Gelman, A., Hoffman, M. D., Lee, D., Goodrich, B., Betancourt, M., Brubaker, M. Guo, J., Li, P., and Riddell, A. 2017. Stan: A Probabilistic Programming Language. J stat. softw. 76:32.

Caswell, H. 2001. Matrix population models: construction, analysis, and interpretation. 2nd ed. Sinauer Associates, Sunderland, MA.

Caughley, G. 1966. Mortality patterns in mammals. Ecology 47:906–18

Chu, C. Y. C., Chien, H. K., and Lee, R. D. 2007. Explaining the optimality of U-shaped age-specific mortality. Theor. Popul. Biol. 73, 171–180.

Colbourne, E., Holden, J., Senciall, D., Bailey, W., Snook, S., and Higdon, J. 2016. Physical Oceanographic conditions on the Newfoundland and Labrador Shelf during 2015. DFO Can. Sci. Advis. Sec. Res. Doc. 2016/079. v +40 p.

Cyr, F., and Galbraith, P.S. 2021. A climate index for the Newfoundland and Labrador shelf. Earth Syst. Sci. Data. 13: 1807-1828

DFO. 2020. 2019 Status of Northwest Atlantic Harp Seals, *Pagophilus groenlandicus*. DFO Can. Sci. Advis. Sec. Sci. Advis. Rep. 2020/020.

Eberhardt, L.L. 2002. A paradigm for population analysis of long-lived vertebrates. Ecology 83:2841-2854.

Fisher, H.D. 1954. Studies on reproduction in the harp seals (*Phoca groenlandica* Erxleben) in the Northwest Atlantic. Ph.D. Thesis Dept., of Zoology, McGill University, Montreal, QC, Canada.

Frie, A.K., Fagerheim, K.-A., Hammill, M.O., Kapel, F.O., Lockyer, C., Stenson, G.B., Rosing-Asvid, A., and Svetochev, V. 2011. Error patterns in age estimation of harp seals (*Pagophilus groenlandicus*): results from a transatlantic, image-based blind-reading experiment using known-age teeth. ICES J. Mar. Sci. 68:1942-1953.

Gelfand, A. E., Ghosh, S. K., Christiansen, C., Soumerai, S. B., and McLaughlin, T. J. 2000. Proportional hazards models: a latent competing risk approach. J. Royal Statist. Soc.: Ser. C (Applied Statistics) 49:385–397.

Gelman, A. 2006. Prior distributions for variance parameters in hierarchical models (comment on article by Browne and Draper). Bayesian Anal. 1:515–534.

Gelman, A., Jakulin, A., Pittau, M. G., and Su, Y.-S. 2008. A weakly informative default prior distribution for logistic and other regression models. Ann. Appl. Stat. 2:1360–1383.

Hammill, M.O., and Sauvé, C. 2017. Growth and condition in harp seals: evidence of density-dependent and density-independent influences. ICES J. Mar. Sci. 74:1395–1407.

Hammill, M.O., and Stenson, G.B. 2009. A preliminary evaluation of the performance of the Canadian management approach for harp seals using simulation studies. DFO Can. Sci. Advis. Sec. Res. Doc. 2009/093. iv + 47 p.

Hammill, M. O. and Stenson, G. B. 2010. Abundance of Northwest Atlantic harp seals (1952-2010). DFO Can. Sci. Advis. Sec. Res. Doc. 2009/114. iv + 12 p.

Hammill, M.O. and Stenson, G. B. 2022. The harp seal: Adapting behavioural ecology to a pack-ice environment. In: D. Costa and E. McHuron (eds). Ethology and Behavioural Ecology of Marine Mammals. Springer International Publishing AG.

Hammill, M.O., Stenson, G.B., Mosnier, A., and Doniol-Valcroze, T. 2014. Abundance estimates of Northwest Atlantic Harp seals and management advice for 2014. DFO Can. Sci. Advis. Sec. Res. Doc. 2014/022. v + 33 p

Hammill, M.O., Stenson, G.B., Doniol-Valcroze, T., and Mosnier, A. 2015. Conservation of northwest Atlantic harp seals: Past success, future uncertainty? Biol. Conserv. 192:181-191.

Hammill, M.O., Stenson, G.B., Mosnier, A., and Doniol-Valcroze, T. 2021. Trends in abundance of harp seals, *Pagophilus groenlandicus*, in the Northwest Atlantic, 1952-2019. DFO Can. Sci. Advis. Sec. Res. Doc. 2021/006. iv + 30 p.

Härkönen, T., Harding, K.C., and Heide-Jørgensen, M.-P. 2002. Rates of increase in age-structured populations: A lesson from the European harbour seals. Can. J. Zool. 80(9): 1498–1510. doi:10.1139/z02-141.

Healey, B.P., and Stenson, G.B. 2000. Estimating pup production and population size of the northwest Atlantic harp seal (*Phoca groenlandica*). DFO Can. Stock Ass. Secr. Res. Doc. 2000/081. 27p.

Heisey, D. M., and Patterson, B. R. 2006. A Review of methods to estimate cause-specific mortality in presence of competing risks. J. Wildl. Manag. 70:1544–1555.

Myers, R.A., and Bowen, W.D. 1989. Estimating bias in aerial surveys for harp seal pup production. J. Wildl. Manag. 53:361-372.

R.Core.Team. 2022. R: A language and environment for statistical computing. R Foundation for Statistical Computing, Vienna, Austria.

Roff, D. A., and Bowen, W. D. 1983. Population dynamics and management of the northwest Atlantic harp seal (*Phoca groenlandica*). Can. J. Fish. Aquat. Sci. 40: 919-932.

Roff, D.A., and Bowen, W.D. 1986. Further analysis sf population trends in the northwest Atlantic harp seal (*Phoca groenlandica*) from 1967 to 1985. Can. J Fish. Aquat. Sci. 43: 553-564.

Rossi, S.P., Cox, S.P., Hammill, M.O., den Heyer, C.E., Swain, D.P., Mosnier, A., and Benoit, H.P. 2021. Forecasting the response of a recovered pinniped population to sustainable harvest strategies that reduce their impact as predators. ICES J. Mar Sci. 78:1804-1814.

Sergeant, D.E. 1975. Estimating numbers of harp seals. Rapp. P.-v. réun., Cons. int. Explor. Mer. 169:274-280.

Sergeant DE 1991. Harp seals man and ice. Can Spec Publ Fish Aquat Sci 114: 153 p.

Sergeant, D.E., and Fisher, H.D. 1960. Harp seal populations in the western North Atlantic from 1950 to 1960. Fish. Res. Board Can. Arctic Unit. Circular No. 5. 58 p.

Sigourney, D.B., Murray, K.T., Gilbert, J.R., Ver Hoef, J.M., Josephson, E., and Digiovanni Jr, R.A. 2021. Application of a bayesian hierarchical model to estimate trends in Atlantic harbor seal (*Phoca vitulina vitulina*) abundance in Maine, U.S.A., 1993-2018. Mar. Mamm. Sci. 38:500-516.

Shelton, P.A., Cadigan, N.G., and Stenson, G.B. 1992. Model estimates of harp seal population trajectories in the Northwest Atlantic. Can. Atlan. Fish. Sci. Adv. Coun. Res. Doc. 92/89. 23p.

Sjare, B., and Stenson, G.B. 2002. Estimating struck and loss rates for harp seals (*Pagophilus groenlandicus*) in the Northwest Atlantic. Mar. Mamm. Sci. 18, 710-720.

Sjare, B., and Stenson, G.B. 2010. Changes in the reproductive parameters of female harp seals (*Pagophilus groenlandicus*) in the Northwest Atlantic. ICES J. Mar. Sci. 67: 304-315.

Sjare, B., Stenson, G.B., and Warren, W. G. 2000. Recent estimates of reproductive rates for harp seals in the Northwest Atlantic. Can. Stock. Ass. Sec. Res. Doc. 2000/077. 13p.

Stenson, G., and Hammill, M.O. 2014. Can ice breeding seals adapt to habitat loss in a time of climate change? ICES J. Mar. Sci. 71:1977–1986.

Stenson, G.B. and Upward, P. 2020. Updated Estimates of Harp Seal Bycatch and Total Removals in the Northwest Atlantic. DFO Can. Sci. Advis. Sec. Res. Doc. 2020/014.

Stenson, G.B., Myers, R.A., Hammill, M.O., Ni, I-H., Warren, W.G., and Kingsley, M.C.S. 1993. Pup production of Harp Seals *Phoca groenlandica*, in the northwest Atlantic. Can. J. Fish. Aquat. Sci. 50:2429-2439.

Stenson, G.B., Hammill, M.O., Kingsley, M.C.S., Sjare, B., Warren, W.G., and Myers, R.A. 2002. Is there evidence of increased pup production in Northwest Atlantic Harp Seals, *Pagophilus groenlandicus*? ICES J. Mar. Sci. 59:81-92.

Stenson, G., Rivest, L., Hammill, M.O and Gosselin, J.F. 2003. Estimating pup production of harp seals, *Pagophilus groenlandicus*, in the Northwest Atlantic. Mar. Mamm. Sci. 19:141–160.

Stenson, G.B., Hammill, M.O., Lawson, J.W., and Gosselin, J.F. 2014. Estimating Pup Production of Northwest Atlantic Harp Seals, *Pagophilus groenlandicus*, in 2012. DFO Can. Sci. Advis. Sec. Res. Doc. 2014/057.v + 43p.

Stenson, G.B., Buren, A.D., and Koen-Alonso, M. 2016. The impact of changing climate and abundance on reproduction in an ice-dependent species, the Northwest Atlantic harp seal, *Pagophilus groenlandicus*. ICES. J. Mar. Sci. 73:250-262.

Stenson, G. B., Buren, A. D., and Sheppard, G. L. 2020a. Updated estimates of reproductive rates in Northwest Atlantic harp seals and the influence of body condition. DFO Can. Sci. Advis. Sec. Res. Doc. 2020/057. iv + 22 p.

Stenson G.B., Haug, T., and Hammill, M.O. 2020b. Harp Seals: Monitors of Change in Differing Ecosystems Front. Mar. Sci. 7:569258. doi: 10.3389/fmars.2020.569258

Stenson, G., Gosselin, JF., Lawson, J., Buren, A., Goulet, P., Lang, S., Nilssen, K.T., and Hammill, M.O. 2022. Pup production of harp seals in the Northwest Atlantic in 2017 during a time of ecosystem change. NAMMCO Sci. Publ. 12.

Vehtari, A., Gelman, A., and Gabry, J. 2017. Practical Bayesian model evaluation using leave-one-out cross-validation and WAIC. Stat.Comp. 27:1413–1432.

Wang, G. 2009. Signal extraction from long-term ecological data using Bayesian and non-Bayesian state-space models. Ecol. Inform. 4:69–75.

Williams, P. J., Hooten, M. B., Womble, J. N., Esslinger, G. G., Bower, M. R., and Hefley, T. J. 2017. An integrated data model to estimate spatiotemporal occupancy, abundance, and colonization dynamics. Ecology 98:328–336.

APPENDICES

Appendix 1, Table A1.1. Age-specific pregnancy rates of female harp seals sampled in Newfoundland and Labrador waters 1954 to 2019 from Stenson et al. (2020a) and used in Hammill et al (2021) and in current paper. Rates are based on the proportion of pregnant females in each particular age class (Stenson et al. 2020a).

Year	Age (y)	# sample	# animal pregnant	Age (y)	# sample	# animal pregnant	Age (y)	# sample	# animal pregnant	Age (y)	# sample	# animal pregnant	Age (y)	# sample	# animal pregnant
1952	4	0	NA	5	0	NA	6	0	NA	7	0	NA	8	0	NA
1953	4	0	NA	5	0	NA	6	0	NA	7	0	NA	8	0	NA
1954	4	4	0	5	3	1	6	3	2	7	16	12	8	33	29
1964	4	11	0	5	9	1	6	2	1	7	4	3	8	25	22
1965	4	30	1	5	44	5	6	37	20	7	38	27	8	109	96
1966	4	7	0	5	9	1	6	17	6	7	11	8	8	49	43
1967	4	10	0	5	19	4	6	33	20	7	29	28	8	123	109
1968	4	27	0	5	19	6	6	20	14	7	12	11	8	55	48
1969	4	25	1	5	25	4	6	16	7	7	28	23	8	165	146
1970	4	13	0	5	13	3	6	12	6	7	10	9	8	107	92
1978	4	40	1	5	38	23	6	20	18	7	9	6	8	0	NA
1979	4	4	1	5	1	1	6	0	NA	7	1	1	8	8	4
1980	4	2	0	5	2	1	6	1	1	7	0	NA	8	12	9
1981	4	5	1	5	4	3	6	2	1	7	7	6	8	17	14
1982	4	4	0	5	5	2	6	1	1	7	4	3	8	3	1
1985	4	4	0	5	3	1	6	5	2	7	3	3	8	1	1
1986	4	1	1	5	0	NA	6	2	1	7	1	0	8	11	8
1987	4	12	2	5	8	3	6	9	7	7	4	4	8	24	15
1988	4	17	2	5	6	1	6	3	3	7	0	NA	8	19	14
1989	4	8	0	5	9	0	6	6	2	7	3	2	8	25	21
1990	4	8	0	5	6	1	6	3	1	7	1	0	8	10	6
1991	4	10	0	5	11	2	6	7	4	7	3	1	8	29	18
1992	4	9	2	5	11	3	6	7	3	7	8	6	8	32	21
1993	4	11	0	5	17	2	6	7	0	7	5	4	8	35	16
1994	4	23	1	5	15	2	6	14	6	7	6	2	8	40	33
1995	4	10	0	5	13	6	6	4	2	7	5	2	8	26	14
1996	4	8	0	5	6	0	6	4	1	7	1	1	8	37	24
1997	4	5	0	5	4	0	6	10	3	7	2	2	8	36	26
1998	4	6	0	5	10	3	6	9	2	7	4	2	8	36	21
1999	4	6	0	5	7	0	6	17	4	7	15	6	8	60	35
2000	4	1	0	5	9	3	6	6	4	7	5	2	8	42	29
2001	4	2	0	5	0	NA	6	2	2	7	3	0	8	39	26
2002	4	2	0	5	4	1	6	5	3	7	16	9	8	71	30
2003	4	1	0	5	3	2	6	2	1	7	3	2	8	90	57
2004	4	2	0	5	5	0	6	5	1	7	1	0	8	77	23
2005	4	9	1	5	9	0	6	13	2	7	7	0	8	86	54
2006	4	2	0	5	0	NA	6	0	NA	7	0	NA	8	119	57
2007	4	1	0	5	5	0	6	3	1	7	2	2	8	84	62

Year	Age (y)	# sample	# animal pregnant	Age (y)	# sample	# animal pregnant	Age (y)	# sample	# animal pregnant	Age (y)	# sample	# animal pregnant	Age (y)	# sample	# animal pregnant
2008	4	6	0	5	3	0	6	2	0	7	0	NA	8	61	43
2009	4	1	0	5	1	0	6	1	0	7	1	1	8	105	59
2010	4	0	NA	5	0	NA	6	0	NA	7	1	0	8	114	35
2011	4	3	0	5	2	0	6	0	NA	7	0	NA	8	153	30
2012	4	2	0	5	1	0	6	0	NA	7	0	NA	8	12	5
2013	4	1	0	5	0	NA	6	0	NA	7	1	0	8	11	6
2014	4	2	0	5	0	NA	6	1	0	7	1	0	8	76	65
2015	4	0	NA	5	1	0	6	0	NA	7	3	0	8	19	15
2016	4	7	0	5	4	1	6	6	2	7	4	3	8	93	69
2017	4	7	0	5	8	0	6	0	NA	7	2	0	8	50	29
2018	4	10	0	5	6	0	6	3	1	7	2	1	8	69	51
2019	4	5	0	5	4	0	6	2	0	7	4	1	8	110	80

Appendix 2: Determining optimal minimum age for inclusion in model fitting

The Stochastic model incorporated age-structure information from the Newfoundland sampling program into the fitting process, enabling the model to converge. Seals of all ages have been collected under a variety of programs designed for different objectives. It is therefore possible that some age groups, mostly likely the younger who do not have adult pelages, may be over or under estimated in age structure.

In the previous assessment, the Deterministic model was fit to the reproductive rates of females 8 years and older and the pup production estimates from the surveys. Animals aged 8 y and older were selected because examination of the pelage type of both males and females indicated that by the age of 8, over 90% of the seals had the full adult or 'spotted harp' pelage and would have been randomly sampled in the collections. Also, the 8+ animals are also very close to maximum size (length and weight) and these animals of 8 yrs or older are very difficult to distinguish based on age. Therefore, samples of these older animals are thought to provide an unbiased age-structure sample of the 'adult' population. This was similar to the findings of Roff and Bowen (1983, 1986) who considered that samples including animals aged 7 years and older represented an unbiased age structure of the population. However, while excluding younger ages from model fitting reduces concerns about potential sampling bias, there is an associated penalty in terms of reduced sample sizes and statistical power. This can be especially problematic when ages are excluded from the bottom end of the age distribution.

Generally, the dynamics of a population are most sensitive to changes in adult survival. However, adult survival tends to be high and shows little inter-annual variation, whereas juvenile survival can vary considerably between years depending on density-dependent and environmental (density-independent) factors. Subsequent changes in cohort strength of younger age classes can have a significant impact on population trends (Caswell 2001; Eberhardt 2002; Harkonen et al. 2002). Excluding younger animals from the analysis (animals 0-6 y old) therefore reduces the model's ability to track changes in juvenile mortality, particularly in the last 5-10 years of the time series, due to the time-lag between when changes are likely to occur (ages 0-6 y) and when they will be detected, as it takes time for them to be fully recruited into the population model (ages 7 y and older).

The Stochastic model utilizes the age distribution data of both males and females obtained as part of the Newfoundland sampling program. A change in the recruitment of younger animals to the population is evident based on a cursory examination of the raw age structure data over time (Figure 6). The younger age classes initially dominated the age structure in the sampled population, but over time the age structure reflected an increasingly ageing population, with samples dominated by animals 16+ years since 2009 (although in some years the sample sizes are small, Figure 6). Juvenile mortality was thought to be extremely high in 2010 and 2011 due to very poor ice conditions (Stenson et al. 2014). This spike of juvenile mortality would not be expected to appear in the model until 2018 with a minimum age of 8, however lower recruitment is apparent by 2014 using a minimum age of 4 years old. Similarly, an increase in juvenile survival over the last 5 years of the data set would not be detectable when the minimum age is 7 or 8 (since those younger ages do not make it into the sample by the end of the time series) but is apparent with minimum age of 4 or 5 (Figure 6).

We ran multiple model fits to explore the impacts of changing the minimum age (m) to be included in the age structure dataset used for model fitting. We used an information theoretic approach to compare models with different values of m (4 – 8 years) to select the best supported model. Specifically, we calculated the "Leave-one-out cross validation information criterion" (LooIC) for each model (using the Loo package in R) and we identified the best supported model based on the lowest LooIC value or (equivalently) the highest expected log

pointwise predictive density (ELPD) for a new data set. Similar to AIC comparisons of models fit by Maximum Likelihood, the Bayesian-based LooIC comparison can be used to identify the best-supported model based on maximizing likelihood while penalizing for additional fitted parameters. LooIC is generally preferred over AIC as it utilizes the full joint posterior, rather than just the point estimate. The model having the lowest LooIC (or highest ELPD) is thus both the most parsimonious and most likely to correctly estimate new data points (or data points excluded from model fitting, via Leave-one-out cross validation).

Varying the minimum age included in model fitting was associated with changes in the estimated values of pup production and abundance, particularly for the years since 2010 (Figure A2.1). In general, as the minimum age was reduced, estimates of pup production and total abundance in 2017 and 2019 increased, while the uncertainty around these estimates decreased (Table A2.1). The best supported model had values of m = 5 years (Table A2.2) This model was used for generating all reported statistics, figures, and derived parameters.

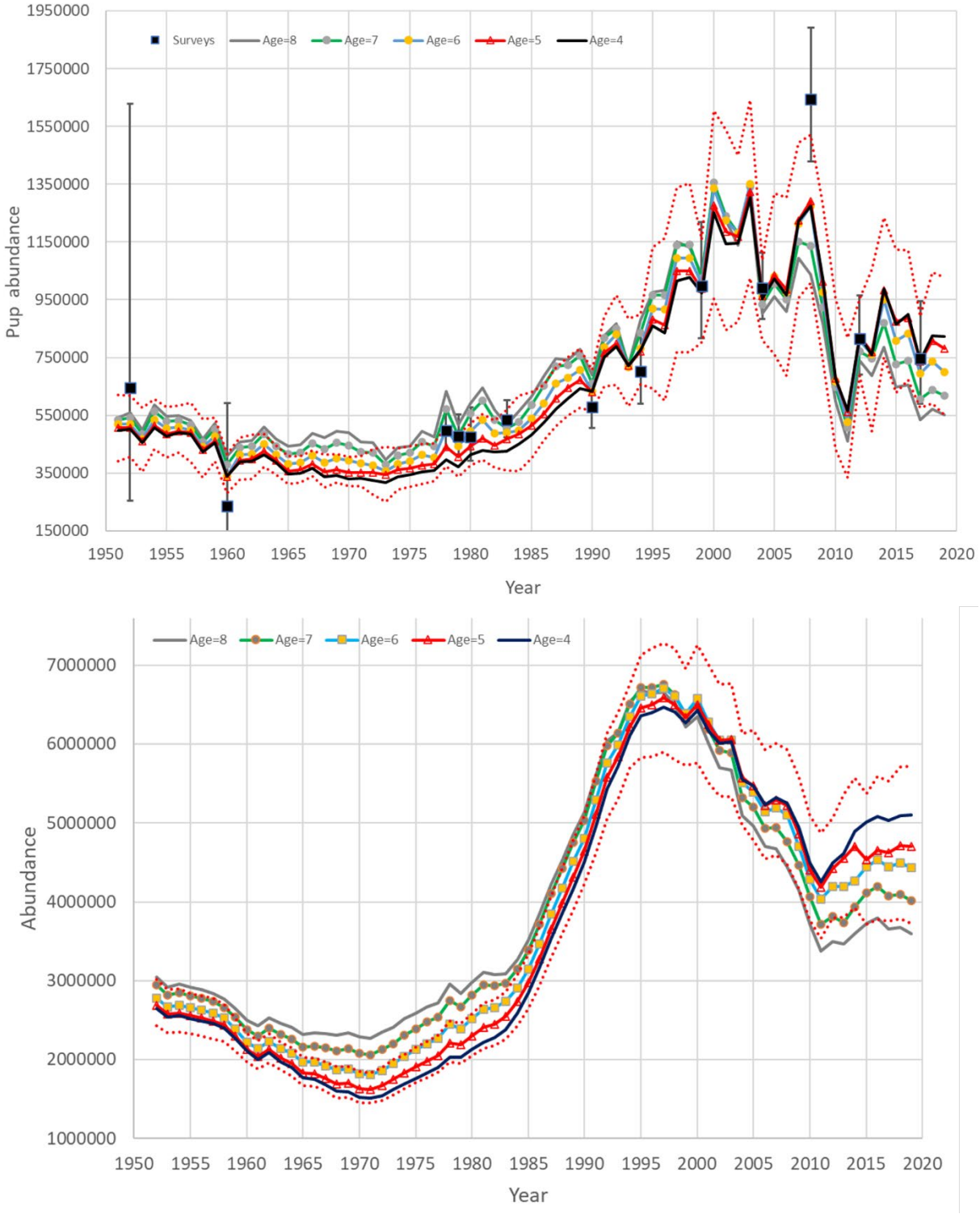

Figure A2.1. Plots showing changes in estimates of pup production (top), total abundance (bottom) with model runs that included different minimum age classes (m) in model fitting. The dotted lines show the 95% credibility intervals for the model runs with m = 5 years (red).

Appendix 2, Table A2.1. Model derived statistics of pup production and total abundance for 2017 and 2019, including estimates of means, coefficients of variation (CV) and 95% Credibility Intervals (95% CI), generated from models fit to data sets with different minimum ages (m) in age distributions. Refer to methods for more details on alternative models. Survey estimates of pup abundance are found in Table 1.

		Estimates			
Min. Age (m)	Statistic	Pup prod., 2017	Pup prod., 2019	Abundance, 2017	Abundance, 2019
5	Mean	735,000	776,000	4,595,000	4,667,000
	CV (%)	11	15	10	11
	CI95_lo	568,000	558,000	3,698,000	3,712,000
	CI95_hi	890000	1,011,000	5,529,000	5,679,000
6	Mean	695,000	700,000	4,443,000	4,434,000
	CV (%)	12	16	11	11
	CI95_lo	518,000	481,000	3,500,000	3,432,000
	CI95_hi	847,000	930,000	5,368,000	5,441,000
7	Mean	606,000	617,000	4,074,000	4,017,000
	CV (%)	18	19	14	14
	CI95_lo	386,000	386,000	2,935,000	2,838,000
	CI95_hi	873,000	873,000	5,126,000	5,100,000
8	Mean	535,000	551,000	3,660,000	3,599,000
	CV (%)	21	21	15	16
	CI95_lo	320,000	337,000	2,551,000	2,432,000
	CI95_hi	751,000	787,000	4,721,000	4,706,000

Appendix 2, Table A2.2. Results of model comparison using "Leav-one-out cross-validation information criterion" (LooIC). The LooIC criteria was used to evaluate relative degree of support for six alternative models, which differed in terms of the minimum age (m) included in the age structure data used for model fitting. The model with minimum LooIC or (equivalently) maximum expected log pointwise predictive density difference (ELPD_Loo) has the greatest likelihood of correctly predicting data points that were excluded from model fitting. Models are sorted based on relative degree of support, as measured by the difference (ELPD_diff) between the associated ELPD_Loo values and that of the best-supported model. Also shown are the standard error of the differences (SE diff), standard error of ELPD_Loo (SE elpd loo), the effective number of parameters (P_loo) and standard error (SE_P_loo), and the standard error of LooIC (SE LooIC).

m	Elpd diff	SE diff	Elpd Loo	SE Elpd Loo	P loo	SE P Loo	LooIC	SE LooIC
5	0.0	0.0	-545.8	46.6	36.3	5.6	1091.6	93.2
4	-1.6	1.7	-547.4	46.9	35.6	5.2	1094.8	93.8
6	-2.0	1.5	-547.7	46.7	38.5	5.7	1095.5	93.4
7	-7.1	2.5	-552.9	47.4	38.7	5.8	1105.8	94.9
8	-9.0	3.5	-554.8	47.3	36.6	4.9	1109.6	94.6

Appendix 3: Reported catches

Table A3.1. Reported catches from commercial and subsistence harvests in the Canadian Arctic (Arctic), Greenland, the Canadian commercial harvest consisting of young of the year (YOY)(Can pup) and animals 1 year and older (Can 1+) and estimated removals from commercial fisheries represented by animals aged 1 year and older (Bycatch Age 1+) and YOY (Bycatch YOY). From Stenson and Upward (2020).

YEAR	Arctic	Greenland	Can pup	Can 1+	Bycatch Age 1 +	Bycatch YOY
1952	1784	16400	198063	109045	0	0
1953	1784	16400	197975	74911	0	0
1954	1784	19150	175034	89382	0	0
1955	1784	15534	252297	81072	0	0
1956	1784	10973	341397	48013	0	0
1957	1784	12884	165438	80042	0	0
1958	1784	16885	140996	156790	0	0
1959	1784	8928	238832	81302	0	0
1960	1784	16154	156168	121182	0	0
1961	1784	11996	168819	19047	0	0
1962	1784	8500	207088	112901	0	0
1963	1784	10111	270419	71623	0	0
1964	1784	9203	266382	75281	0	0
1965	1784	9289	182758	51495	0	0
1966	1784	7057	251135	72004	0	0
1967	1784	4242	277750	56606	0	0
1968	1784	7116	156458	36238	0	0
1969	1784	6438	233340	55472	0	0
1970	1784	6269	217431	40064	17	60
1971	1784	5572	210579	20387	85	440
1972	1784	5994	116810	13073	141	481
1973	1784	9212	98335	25497	107	361
1974	1784	7145	114825	32810	42	141
1975	1784	6752	140638	33725	66	220
1976	1784	11956	132085	32917	169	926
1977	1784	12866	126982	28161	309	1324
1978	2129	16638	116190	45533	613	2763

YEAR	Arctic	Greenland	Can pup	Can 1+	Bycatch Age 1 +	Bycatch YOY
1979	3620	17545	132458	28083	572	3031
1980	6350	15255	132421	37105	274	2540
1981	4672	22974	178394	23775	406	3775
1982	4881	26927	145274	21465	347	3470
1983	4881	24785	50058	7831	462	4547
1984	4881	25829	23922	7622	429	3714
1985	4881	20785	13334	5701	642	4345
1986	4881	26099	21888	4046	896	5213
1987	4881	37859	36350	10446	1864	9047
1988	4881	40415	66972	27074	1406	6993
1989	4881	42971	56346	8958	726	7918
1990	4881	45526	34402	25760	795	1974
1991	4881	48082	42382	10206	608	8094
1992	4881	50638	43866	24802	6411	16624
1993	4881	56319	16401	10602	7732	19244
1994	4881	57373	25223	36156	10836	36768
1995	4881	62749	34106	31661	6341	14252
1996	4881	73947	184856	58050	18745	10896
1997	2500	68816	220476	43734	5188	13860
1998	1000	81262	251403	31221	973	3584
1999	500	93117	237644	6908	6325	9843
2000	400	98462.5	85035	7020	1632	9890
2001	600	85427.5	214754	11739	4992	15072
2002	1000	66734.5	297764	14603	3901	5642
2003	1000	66149	280174	9338	1912	3533
2004	1000	70586.5	353553	12418	11228	24642
2005	1000	91687.5	323800	6029	8284	18094
2006	1000	94033.5	346426	8441	5526	16130
2007	1000	82825.5	221488	3257	2990	6460
2008	1000	80444	217565	285	2360	4920
2009	1000	71861.5	76688	0	972	1303

YEAR	Arctic	Greenland	Can pup	Can 1+	Bycatch Age 1 +	Bycatch YOY
2010	1000	89905	68654	447	1338	2618
2011	1000	73462	40371	18	712	1402
2012	1000	54659.5	71319	141	812	2074
2013	1000	65241	94310	3612	27	150
2014	1000	63028	59616	50	214	952
2015	1000	61767	35302	80	196	844
2016	1000	55520	61016	7344	139	464
2017	1000	47515.5	70270	11472	53	173
2018	1000	58614.3	56135	4887	161	450
2019	1000	58614.3	29913	2125	148	563

Appendix 4: Evaluation of uncertainty in reported catches.

There is an unknown level of uncertainty in the reported takes. We examined the impact of uncertainty on parameter estimates by adjusting the coefficient of variation around reported removals (CV=0.0, 0.05, 0.10, 0.20) and running the model with the new estimates. Overall, assuming different levels of uncertainty around the reported removals had no impact on parameter estimates of abundance and trend. The model responded to changes in uncertainty by varying how much mortality it allocated to removals, ice and climate conditions and stochastic mortality. Since it is probable that there is some variation in the reported catches, a CV of 10% was adopted for model runs.

Figure A4.1. Plot showing temporal variation in model-estimated harvest/bycatch removals for adults and YOY (juveniles), with observed data plotted for comparison (model estimates adjusted for struck and loss). Reported harvests assume either no uncertainty (CV=0%) (top-left), or an uncertainty of 5% (top right), 10% (bottom left) and 20% (bottom right) in reported numbers. Solid lines indicate mean estimated values and shaded bands indicate the associated 95% CI.

Figure A4.2. Plot showing relative contributions of various sources of mortality to the total combined mortality rate for YOY (juveniles). Mortality factors compared include removals from harvesting, poor ice conditions, climate effects, and baseline plus density-dependent mortality (including stochastic variation). The dashed line indicates what the expected value of baseline plus density-dependent mortality would be if stochastic variation were excluded. Partitioning of mortality assuming either no uncertainty (CV=0%; top-left), or an uncertainty of 5% (top right), 10% (bottom left) and 20% (bottom right) in reported numbers.

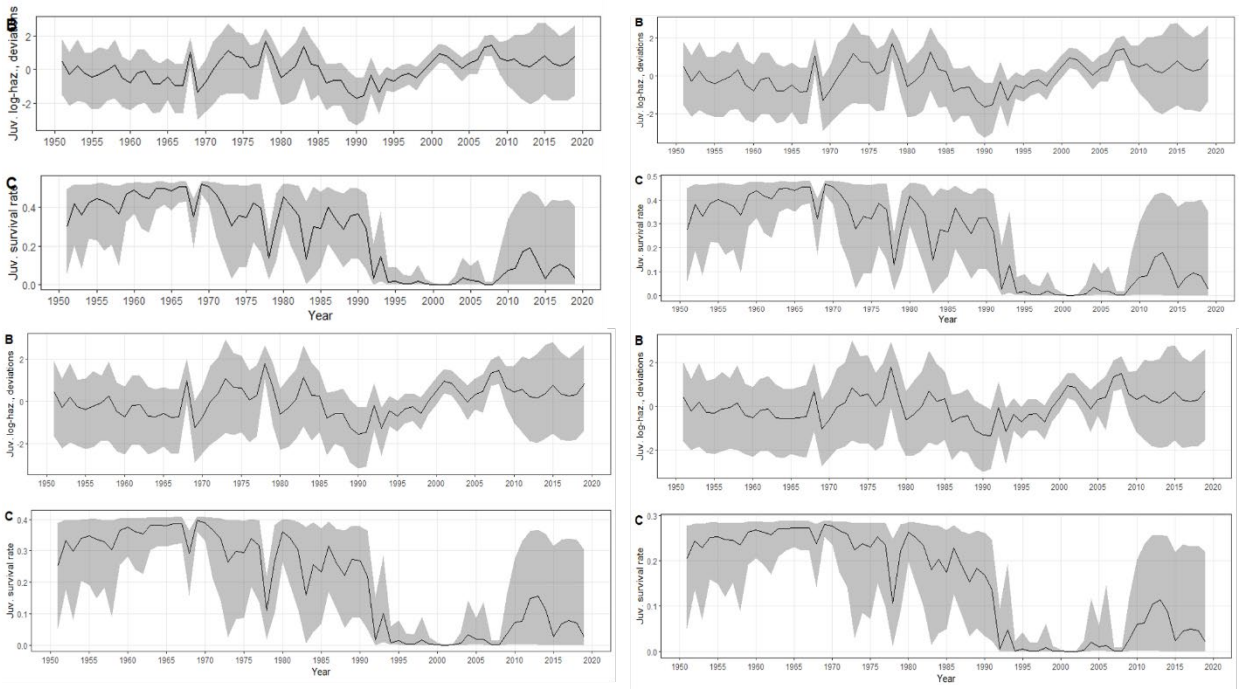

Figure A4.3 Plots showing stochastic variation over time in model-estimated juvenile survival rates: B) deviations from expected log hazard rates for young of the year (YOY); C) realized juvenile survival (including stochastic deviations). Solid lines indicate mean estimated values and shaded bands indicate the associated 95% CI, with an assumed uncertainty (CV) of 0% (top-left), 5% (top-right), 10% (bottom-left) and 20% (bottom-right) in removals.

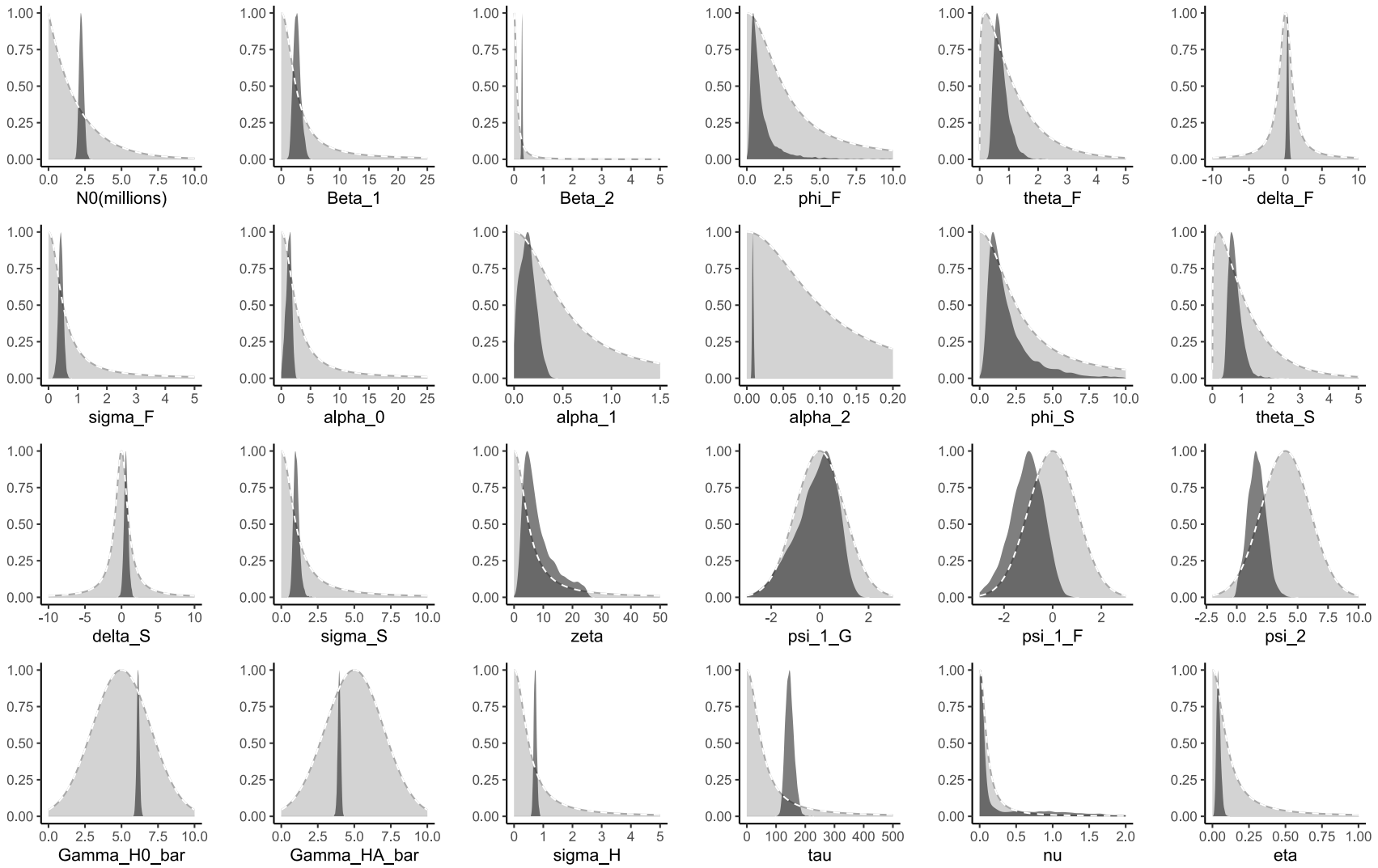

Appendix 5. Figure A5.1. Comparison of prior distributions (light grey shaded areas) to posterior distributions (ark grey shaded areas) for model parameters.